UNIVERSITY OF OKLAHOMA

GRADUATE COLLEGE

INTEGRATED MODELING AND SIMULATION OF MULTI-STAGE HYDRAULIC FRACTURED WELLS IN THE WOODFORD SHALE

A THESIS

SUBMITTED TO THE GRADUATE FACULTY

in partial fulfillment of the requirements for the

Degree of

MASTER OF SCIENCE

By

ANY CLARISETH ORDOÑEZ BUSTAMANTE
Norman, Oklahoma
2019

INTEGRATED MODELING AND SIMULATION OF MULTI-STAGE HYDRAULIC FRACTURED WELLS IN THE WOODFORD SHALE

A THESIS APPROVED FOR THE
MEWBOURNE SCHOOL OF PETROLEUM AND GEOLOGICAL ENGINEERING

BY

Dr. Zulfiquar Reza, Chair

Dr. Roger Slatt

Dr. Hamidreza Karami

To my beloved family for their unconditional support: mamá, papá, abuela y hermanos.

Acknowledgments

I would like to express my deepest appreciation to my advisor, Dr. Zulfiquar Reza, for his guidance, dedication, and encouragement through this work and my graduate studies at the University of Oklahoma. This thesis would not have been possible without his valuable expertise and constant support.

I extend my gratitude to Dr. Roger Slatt and Dr. Hamidreza Karami for serving on my committee, providing valuable feedback on my thesis, and contributing to my professional development throughout their lectures.

I would also like to thank those who collaborated and contributed generously to this work. Thanks to Carlos Molinares, Richard Brito, Javier Tellez, Karelia La Marca, and Maria Fernanda Hurtado, for their input to the geologic aspects of this study. Thanks to Tien Phan, Yuliana Zapata, Saurabh Sinha, Vladimir Vazquez, Johanna Fernandez, and Barbara Chichiricco, for their valuable insights regarding the engineering aspects of this thesis. Thanks to the MPGE faculty and staff for their assistance and support. Thanks to Schlumberger, MathWorks, and Barree and Associates for donating the software licenses used in this study.

Finally, my heartfelt gratitude to my beloved family and friends for their unconditional support and encouragement during this amazing journey. Thanks to Clara, Jesus, Reyna, Oscar, Mayra, Albert, Adrian, Carelia, Elia, Andrea, Michael, Felipe, Laura, Ruben, Mijin, Yao, Marisol, Anna Maria, and all other friends who supported me to accomplish my goals during my master's degree.

Table of Contents

List of Tables

List of Figures

Abstract

The Late Devonian-Early Mississippian Woodford shale is known as the main source rock in the state of Oklahoma, and one of the most attractive unconventional plays in the U.S. Early Woodford's exploration and development was primarily focused on gas-rich plays, especially those in the Arkoma Basin. Nonetheless, liquid-rich plays have been rapidly emerging in recent years. The liquid-rich SCOOP (South Central Oklahoma Oil Province) play within Oklahoma's Anadarko Basin has become of great interest for oil companies due to its noteworthy production of oil and condensates.

The Woodford shale is categorized as an organic-rich siliceous shale and consists of alternating beds of fissile and non-fissile shales with cherty beds. Its varying thickness intervals and variable stratigraphy make it one of the most complex shales in North America. High treatment pressures and fracture gradients, proppant flowback, and pressure-dependent leakoff are some of the factors that have a significant impact on the success of the fracturing treatments in the Woodford. Hence, for the economic development of the Woodford, or any other shale play, it is important to be able to predict and evaluate well performance accurately considering all possible outcomes. The scope of this study is to integrate geologic and hydraulic fracture models to accurately predict and evaluate production performance of multi-stage hydraulic fractured well in the SCOOP play of the Woodford shale.

A 3D static reservoir model was built based on log data from eight wells located in Grady County, Oklahoma. Interpretations from outcrops and previous studies were also used to create the stratigraphic/structural framework. Principal component analysis (PCA) and k-means clustering techniques were implemented to classify rock types and generate the lithofacies model using Sequential Indicator Simulation (SIS). Petrophysical and geomechanical properties were estimated

from well log data and modeled using Sequential Gaussian Simulation (SGS). The resulting geomechanical model was used as input for hydraulic fracture modeling. Eight stimulation treatment designs were evaluated on a single horizontal well to understand the impact of key factors, such as stress, proppant type, and pressure-dependent leakoff on the resulting stimulated reservoir volume. Lastly, the geologic and hydraulic fracture models were coupled into a numerical reservoir simulator to predict and evaluate well performance.

This study illustrated the importance of reservoir characterization and geomechanical modeling for hydraulic fracture design and well performance evaluation. The 3D geologic model confirmed the lateral and vertical heterogeneity of the Woodford shale and its adjacent formations within the study area. The stratigraphic variability captured in the model had an impact on the geomechanical properties and hydraulic fracture modeling. Total stress, pressure-dependent leakoff, and proppant type demonstrated to have a significant effect on the stimulated reservoir volume size and fracture conductivity. Additional work should be performed to understand the coupling of geomechanics and reservoir simulation further.

Chapter 1: Introduction

The Late Devonian-Early Mississippian Woodford shale extends from southern Kansas, through Oklahoma, and into West Texas. Traditionally known as the main source rock in the state of Oklahoma, has now become one of the most attractive unconventional plays in the U.S. Early Woodford developments were focused on gas-rich plays, especially those in the Arkoma Basin. But liquid-rich plays have been emerging rapidly in recent years. The main oil-producing areas of the Woodford are the SCOOP and STACK plays within the Anadarko and Ardmore basins in Oklahoma, along with the Marietta Basin play in North Texas.

The Woodford is considered an organic-rich siliceous shale. It consists of alternating beds of chert and silica-rich shales of varying thickness. The stratigraphic and mineralogy variability makes it one of the most complex shales in North America. This complexity impacts significantly well's productivity. Several studies have been published about the Woodford shale. Most of them focused on structural/stratigraphic characterization, its relationship with geomechanical and geochemical properties, and its role on completion/production strategies. However, few integrated modeling and simulation studies have been published, especially related to the oil-rich plays. This study aims to further understand the complexity of the Woodford's hydraulic fracture network and its impact on production performance.

1.1 Objectives

The main objectives of this study are:

- Build reliable 3D geological and geomechanical models that capture the stratigraphic and petrophysical variability of the Woodford shale and its adjacent formations within the study area.

- Evaluate the effect of certain design parameters on the resulting stimulated reservoir volume by performing hydraulic fracture modeling using the geomechanical model as a constraint.
- Obtain valuable insights regarding the well production performance by coupling the hydraulic fracture model with the geological model.

1.2 Outline

This study is organized as follows. A summary of previous studies and main challenges concerning the development of the Woodford shale is discussed in Chapter 2, as part of the literature review. Chapter 3 presents the methodology used to build a reliable static model of the Woodford and its neighboring formations. A description of the study area and well log data analysis are also shown. Chapter 4 explains the workflow and data used to model asymmetric hydraulic fractures based on the geomechanical model introduced in Chapter 3, as well as the impact of different treatment designs on fracture geometry. Chapter 5 describes the integration of the geologic and hydraulic fracture models in a dual porosity simulation to predict well production performance. Important observations and encountered limitations are addressed in Chapter 6. Lastly, the most important outcomes of this study are listed in Chapter 7.

Chapter 2: Literature Review

The Late Devonian-Early Mississippian Woodford shale is known as the main source rock in the state of Oklahoma, and one of the most attractive unconventional plays in the U.S. Early Woodford studies and developments were primarily focused on gas-rich plays, especially those within the Arkoma Basin. But liquid-rich plays have been rapidly emerging in recent years. Main oil-producing areas of the Woodford are the SCOOP and STACK plays within the Anadarko and Ardmore basins in Oklahoma, along with the Marietta Basin play in North Texas.

The Woodford is defined as an organic-rich siliceous shale and consists of alternating beds of fissile and non-fissile shales with cherty beds. It sits over an unconformity with underlying carbonates and shales, and it was deposited in a variety of environmental settings (Callner, 2014; Slatt et al., 2015). The formation most commonly has been divided into three members: upper, middle, and lower, based on lithology and well log response, although more detailed subdivisions have been proposed (McCullough, 2014 and others). Varying thickness intervals with variable stratigraphy makes it one of the most complex shales in North America.

Several studies have provided useful insights about the stratigraphic, lithological, mineralogy, and petrophysical variability of the Woodford. Turner (2016) investigated the stratigraphic cyclicity of the Woodford by combining chemostratigraphy and palynostratigraphy analyses. Galvis-Portilla (2017) identified argillaceous shale, siliceous shale, siliceous mudstone, chert, and dolomitic mudstone as the main lithofacies within the Woodford. Becerra (2017) analyzed the mineral/elemental composition of multiple outcrop samples and related that to mechanical properties, finding relatively ductile intervals are associated with high TOC and clay-rich lithofacies, and relatively brittle intervals are associated with low TOC and quartz-rich lithofacies. Several researchers investigated the origin and characterization of natural fractures

using outcrop data and found that natural fractures density within the Woodford decreases from cherty/silica-rich intervals to organic-rich intervals and, usually, thinner beds have higher fracture density than thicker beds (Ataman, 2008; Badra, 2011; Ghosh, 2017). Abouelresh and Slatt (2011) combined sequence stratigraphy and geomechanics to map the expected hydraulic fracture length at different scales using Woodford and Barnett shale examples. Molinares et al. (2016) and Sierra et al. (2010) investigated the effect of anisotropy on rock strength and concluded that brittle intervals with more laminations (anisotropy) would break more easily when stress is applied parallel to the laminae orientation. Gupta et al. (2013) and Ryan (2017) correlated petrophysical properties with mineralogy and reservoir quality.

The successful development of the Woodford, like any other unconventional play, relies on the effectiveness of the hydraulic fracture treatment and the size of the stimulated reservoir volume (SRV). The Woodford shale has the characteristics to create a complex fracture network, as illustrated in Figure 1 (McKeon, 2011). However, it requires an accurate fracturing design to achieve high completion efficiencies. High pressures and fracture gradients are usually observed within the Anadarko basin wells, where the depth ranges from 11,000 to 14,000 ft. Proppant flowback is a common issue due to high closure stresses (Vulgamore et al., 2018), and significant fluid leakoff due to the opening of pre-existing natural fissures has also been identified throughout diagnostic fracture injection tests (DFIT).

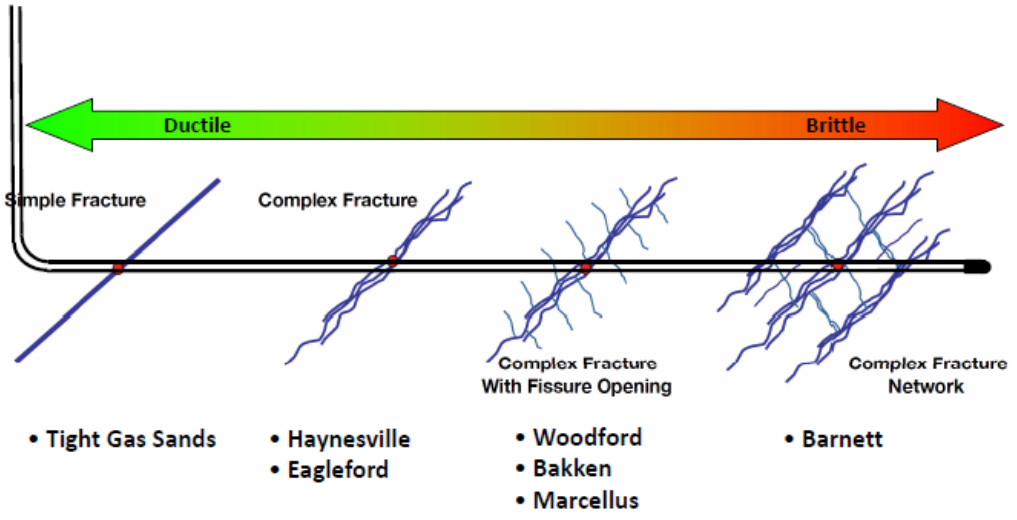

Figure 1. Shale fracture characteristics (modified from (McKeon, 2011)).

Grieser (2011) analyzed 5,000 completion stages in the Oklahoma Woodford and summarized the strategies that appear to have improved the stimulation treatment efficiency. Some of those strategies include: a) the use of slickwater with friction reducer or linear guar gel for better proppant transport; b) an increase in the number of stages along with fewer clusters per stage; c) injection of more volume of fluid and proppant agents at relatively high pumping rates; d) use of curable resin-coated sand to increase conductivity and reduced proppant flowback; and e) pumping of proppant ramp slugs with the initial pad to reduce pressure-dependent leakoff.

Prediction and evaluation of well performance are also important factors in the economic development of unconventional shale resources (Ahmed et al., 2017). Some of the approaches used to forecast production in unconventional wells include decline curve analysis, analytical modeling, and numerical reservoir simulation. The first two options present some limitations regarding the understating of the stimulated volume and pressure depletion profile. Numerical reservoir simulation overcomes those limitations but requires accurate models that represent the reservoir geology and hydraulic fracture size. Few studies about integrated reservoir characterization,

modeling, and simulation within the Woodford shale have been published so far (Peza et al., 2014; Torres-Parada et al., 2018). Therefore, this study aims to integrate geologic and hydraulic fracture models in order to predict and evaluate well performance accurately.

Chapter 3: Reservoir Characterization and Modeling

This chapter discusses the methodology and data used to build a 3D static reservoir model of the Woodford Shale and its neighboring formations, Sycamore Limestone and Hunton Group using Petrel™, an exploration and production software platform. This model aims to combine subsurface data and outcrop/core interpretations from previous studies to capture the reservoir structure, heterogeneity, and properties distribution. Results are presented at the end of the chapter. The 3D static model will then be used as input for multi-stage hydraulic fracture modeling and reservoir simulation of a single horizontal well.

3.1 Stratigraphic/Structural framework

Subsurface data from eight wells in the study area, including gamma ray, bulk density, neutron porosity, and sonic logs were used to build the 3D structural reservoir model. The well logs were available in the form of raster logs, so previous digitalization was performed. Regionally, the study area is located within the SCOOP play of Oklahoma's Anadarko Basin, specifically in Grady County (Figure 2). In this area, the Woodford Shale overlies an erosional unconformity at the top of the Hunton Group and underlies the Sycamore Limestone as highlighted in Figure 3.

The thickness of the Woodford Shale within the Anadarko Basin is variable, with the thickest intervals in the southern part of the basin (Higley, Cook, and Pawlewicz, 2018). The Woodford Shale is most commonly subdivided into three members: upper, middle, and lower. The lower section has the smallest areal extent of the three members, and it's mainly composed by clay-rich and fissile shale, with few interbedded chert and dolomitic beds. The middle section has the greatest areal extent, commonly exhibits the highest radioactivity and contains the highest amount of total organic carbon (TOC). The upper section tends to be the thinnest interval within the south part of the basin, contains several cherty beds interbedded with fissile shale of variable

clay content and contains characteristic phosphate nodules (Becerra, 2017; Galvis-Portilla, 2017; Lambert, 1993; Slatt, 2013).

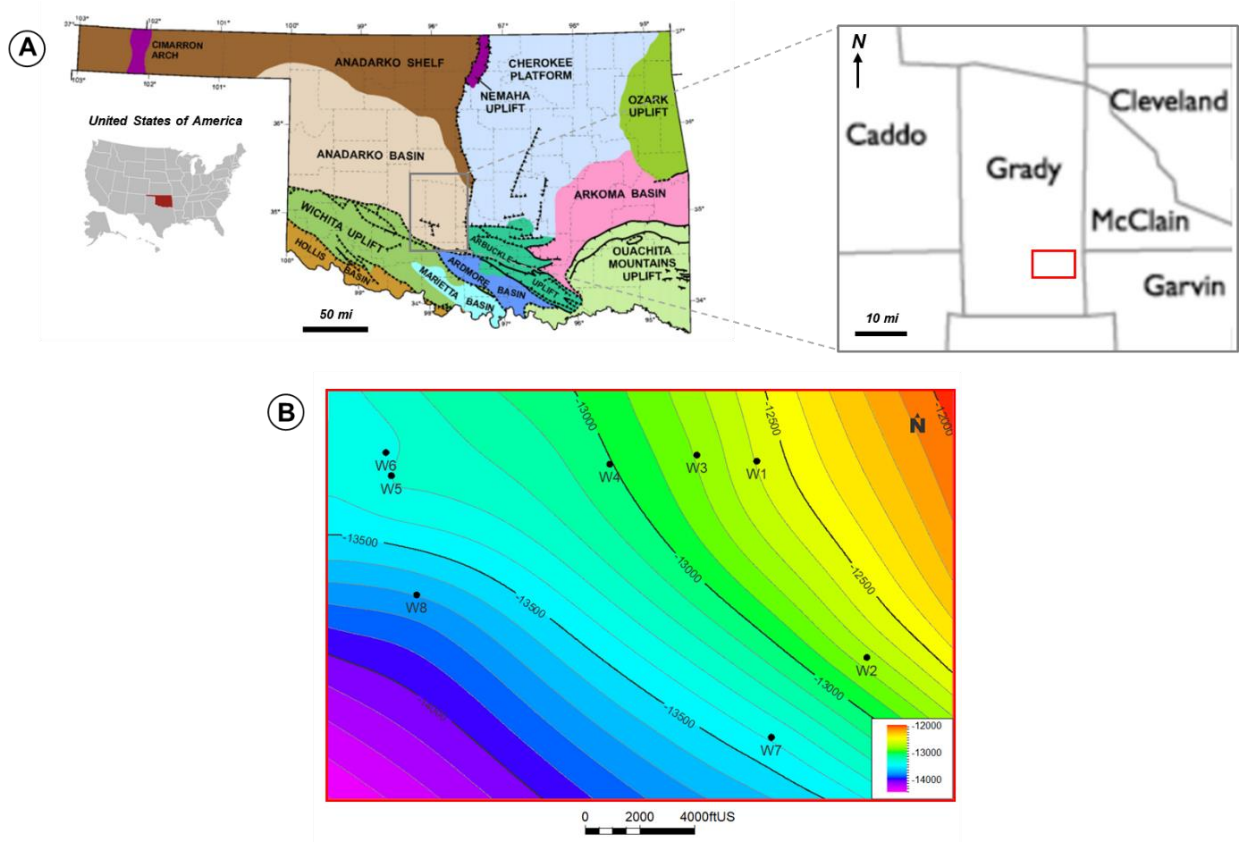

Figure 2. Location of the study area. (A) Oklahoma's Geological provinces map emphasizing the southeast part of the Anadarko Basin and the study area in red (modified from (Cardott, 2012)). (B) Location of the wells overlain by a structural map of the Woodford Shale.

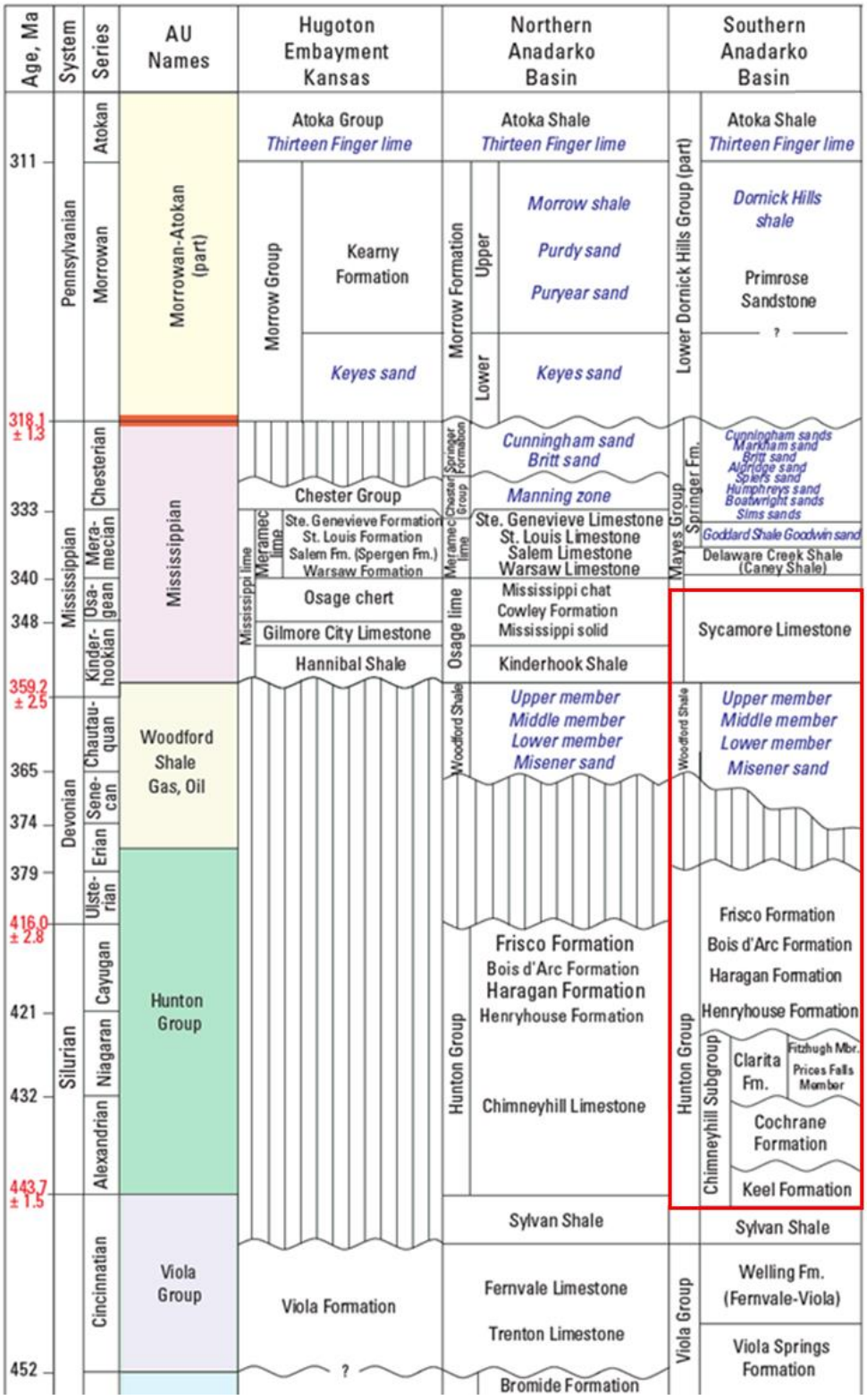

Figure 3. Generalized stratigraphic column for the Anadarko Basin with the study area highlighted in red (modified from (Higley et al., 2018)).

In this study, the structural 3D model encompasses an area of 4.4 x 3 miles (7 x 4.7 Km) and vertically is divided into five zones. The upper and lower zones represent the Sycamore and Hunton formations. The three intermediate zones represent the individual members of the Woodford. The formation tops were picked manually by correlating well-log signatures. Tops of both the Hunton and Woodford are easily identified by the abrupt changes in the gamma-ray log response. These sharp breaks in lithology are usually associated with unconformities and sequence boundaries. Tops of the middle and lower Woodford members were identified by correlating the typical log signatures and lithologic characteristics related to each member. Top of the Sycamore and base of the Hunton were defined to be around 200 and 300 ft from the Woodford, respectively. Figure 4 shows an east-west cross-section with the formation tops and the stratigraphic correlation between two wells within the study area.

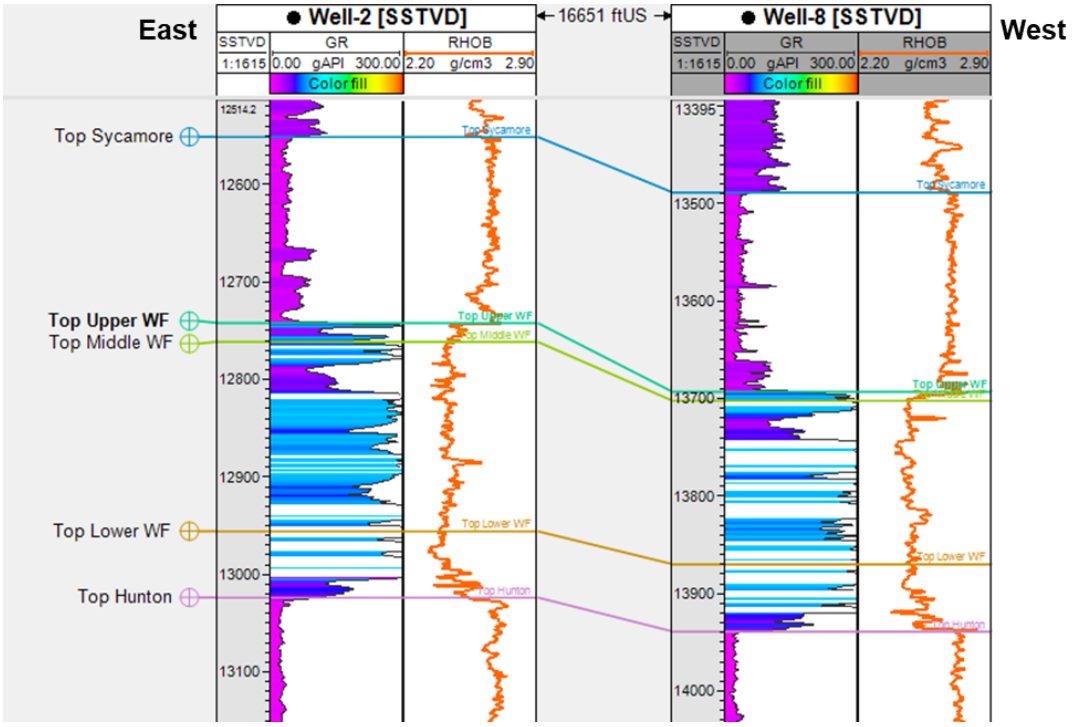

Figure 4. Eas-west cross-section showing the formation tops and the stratigraphic correlation between two wells within the study area.

3.2 Lithofacies classification

In reservoir modeling, Principal Component Analysis (PCA) and k-means clustering are statistical methods usually used to classify lithofacies based on well log data. The PCA technique enables reducing multidimensional datasets by transforming the data into a new orthogonal coordinate system while keeping as much information as possible (Jolliffe, 2002). The new coordinate system has a new set of variables called Principal Components (PC). These principal components, or coordinate axes, are uncorrelated and ordered in such a way that the highest variance of the data is represented by the first principal component, the second-largest variance is represented by the second component, and so on. Consequently, the most important information of all the original variables is contained within the first few principal components, which makes it easier to analyze and cluster different types of data.

In this study, PCA was performed for each formation using log data from five wells. Included well logs are gamma ray (GR), bulk density (RHOB), neutron porosity (NPHI), and compressional sonic travel time (DTC) logs. MATLAB® programming language was used to implement the PCA and clustering workflow. A total of 2,541 data points were used for clustering lithofacies within the Woodford shale interval, 1,974 data points for the Sycamore, and 2,841 data points for the Hunton. Table 1 shows the percentage of the total variation of each principal component for each formation. As a rule of thumb, a cumulative percentage of the total variation of more than 80-90% is considered a good representation of the data (Jolliffe, 2002). In the Woodford, the first three principal components explained 95% of the variance in the data, while in the Sycamore, the first two principal components explained 90% of the variance. Thus, a four-variable analysis is reduced to a three- and a two-variable analysis, respectively.

Table 1. Percentage of the total variation of each principal component for the Woodford shale, Sycamore formation, and Hunton Group.

	Woodford	Sycamore	Hunton
PC1	46.1%	72.2%	49.7%
PC2	30.6%	18.2%	25.1%
PC3	18.8%	5.9%	15.3%
PC4	4.5%	3.6%	9.9%

Woodford lithofacies were grouped into four different clusters using the first three principal components and k-means clustering technique. Similarly, lithofacies for both the Sycamore and Hunton were divided into two main clusters. Figure 5 to Figure 7, show boxplots with the distribution of GR, RHOB, NPHI, and DTC values for each identified cluster in the Woodford, Sycamore, and Hunton intervals, respectively. Each cluster represents a rock type with similar characteristics and depositional environment. Hence, lithofacies were classified by correlating the log data distribution of each rock type with outcrop and core interpretations from previous studies.

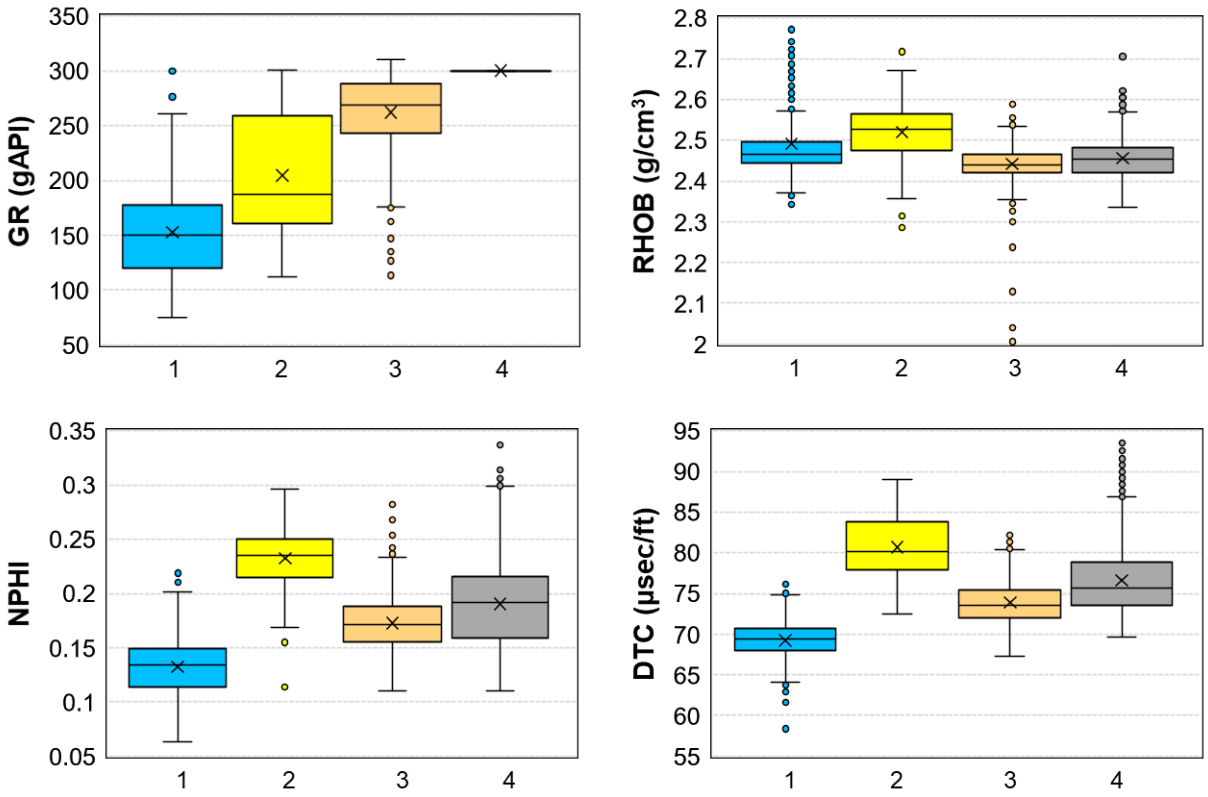

Figure 5. Distribution of GR, RHOB, NPHI, and DTC values for cluster #1 (n=173), cluster #2 (n=365), cluster #3 (n=911), and cluster #4 (n=1092) in the Woodford Shale. n = number of samples analyzed.

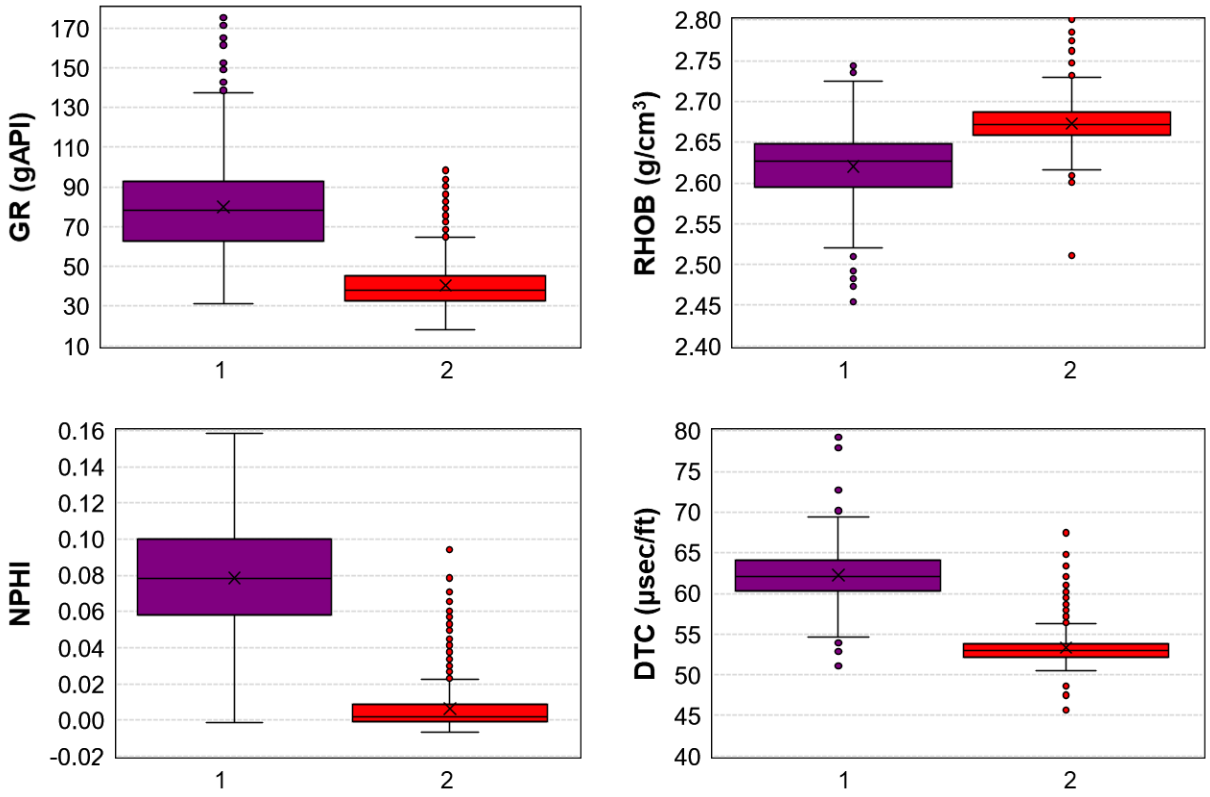

Figure 6. Distribution of GR, RHOB, NPHI, and DTC values for cluster #1 (n=539), and cluster #2 (n=1435) in the Sycamore formation. n = number of samples analyzed.

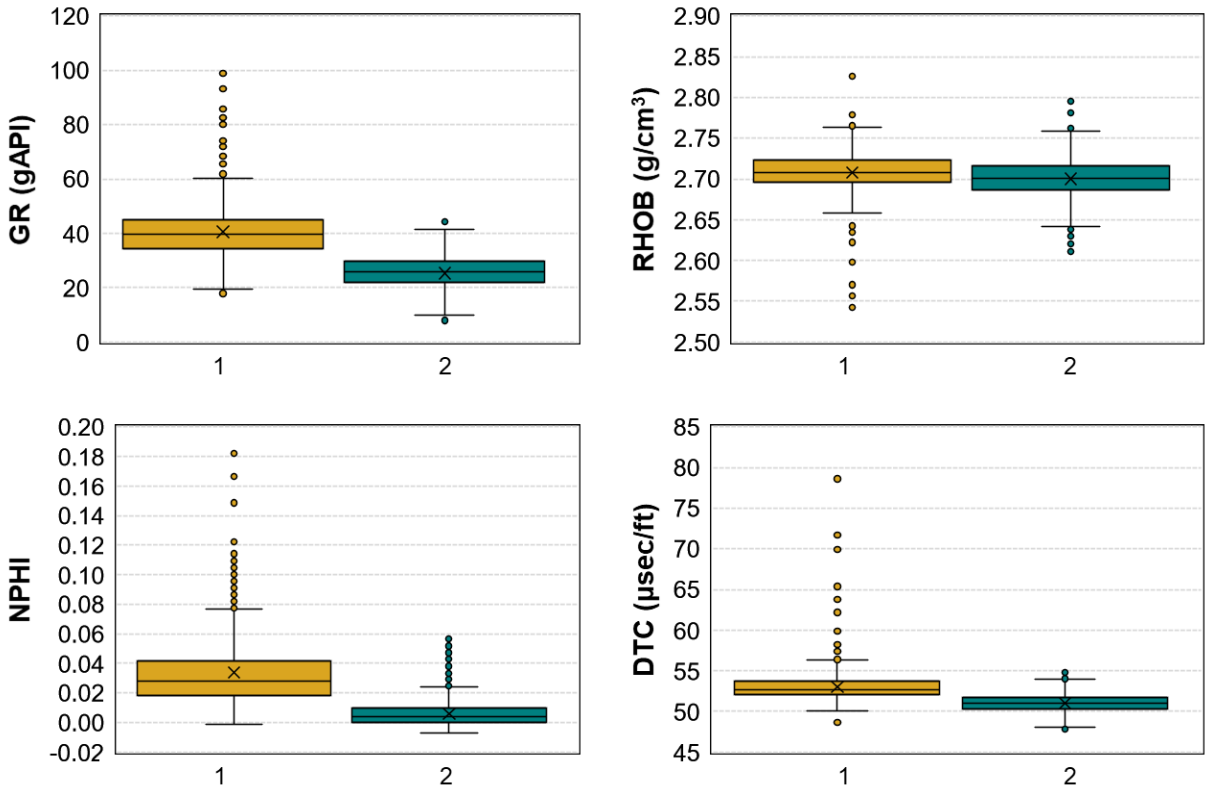

Figure 7. Distribution of GR, RHOB, NPHI, and DTC values for cluster #1 (n=949), and cluster #2 (n=1892) in the Hunton formation. n = number of samples analyzed.

3.2.1 Woodford Shale

Galvis-Portilla (2017) identified the seven most dominant lithofacies within the Woodford Shale using over 550 samples from an outcrop located about 40 miles southeast of the study area. Figure 8 displays the proportion in which those lithofacies identified by Galvis-Portilla (2017) are present within the entire Woodford interval, along with the relative proportion of clays, quartz, and carbonates of each lithofacies. After correlating these with the log response shown in Figure 5 for each rock type, lithofacies in the Woodford shale were classified as follows:

- Dolomitic Mudstone/Shale (Rock Type 1): is the lithofacies with the highest content of carbonates (> 10%). This lithofacies displays low GR, NPHI, and DTC values, but a relatively high RHOB.

- Chert (Rock Type 2): comprises the lithofacies with the highest amount of quartz, typically more than 90%. Cherts are characterized by having a relatively low GR (150-250 gAPI), but high NPHI, DTC, and RHOB.
- Siliceous Mudstone (Rock Type 3): is the second most quartz rich-lithofacies and shows higher GR values compared to Cherts. It also shows intermediate NPHI, RHOB, and DTC values.
- Argillaceous/Siliceous Shale (Rock Type 4): comprises the lithofacies with the highest amount of clay (> 25%). It's characterized by having the highest GR, variable RHOB, and relatively high NPHI values. It includes the black argillaceous shale, black siliceous shale, brown siliceous shale, and siliceous dolomitic shale lithofacies identified by (Galvis-Portilla, 2017).

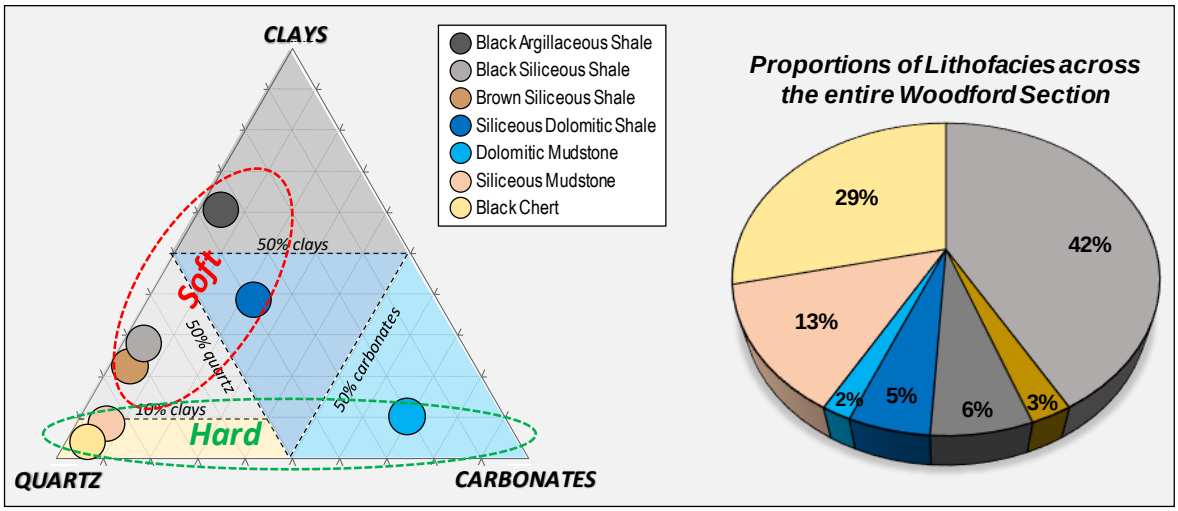

Figure 8. Seven most dominant lithofacies across the Woodford Shale interval identified by Galvis-Portilla (2017). Left: relative proportion of clays, quartz, and carbonates of each lithofacies. Right: percentage of each lithofacies in the entire Woodford section (from (Galvis-Portilla, 2017)).

3.2.2 Sycamore limestone

Miller (2018) identified three dominant lithofacies in the Sycamore formation by the analysis of hand samples and thin sections in an outcrop at the south flank of the Arbuckle Anticline, about 46 miles from the study area. These lithofacies include 1) calcareous siltstone, 2) cherty mudstone, and 3) thinly bedded shale. Rock types in the Sycamore were classified as follows by correlating these lithofacies with log signatures in Figure 7:

- Cherty Mudstone (Rock Type 1): comprises the lithofacies with clay-sized quartz grains. It has intermediate GR, NPHI, and DTC values.
- Calcareous Siltstone (Rock Type 2): represents the lithofacies with silt-sized quartz grains and a high content of calcite cement. Compared to the cherty mudstone, calcareous siltstones show lower GR, NPHI, and DTC values, but higher average RHOB.
- Thinly bedded shales were not observed within the Sycamore interval in the study area.

3.2.3 Hunton Group

Milad (2019) identified wackestone, mudstone, and mud-dominated wackestone as the three main lithofacies in the Hunton Group using well log, seismic, and outcrop data. By correlating these lithofacies with the well-log response in Figure 7, rock types in the Hunton formation were classified as follows:

- Wackestone (Rock Type 2): comprises the mud-supported carbonate rocks that contain more than 10% grains. Compared to the Mud-dominated Wackestone, it displays a lower GR and NPHI signature.
- Mud-dominated Wackestone (Rock Type 1): is very similar to Wackestone, but with higher mud content denoted by a higher GR response.
- Mudstones were not observed within the Hunton interval in the study area.

3.3 Lithofacies modeling

Unconventional shale resources are usually laterally continuous but highly heterogeneous stratigraphically. Due to its depositional processes, lithofacies are commonly stacked in systematic patterns with a cleaning upward gamma-ray signature (Abouelresh and Slatt, 2011; Slatt, 2013). In an attempt to capture as much variability as possible, the 3D grid used to model the Woodford shale has grid cells of 40x40 ft horizontally, and 2 - 4 ft vertically. The total size of the grid is 577x390x175 cells.

Based on the classification presented earlier, a discrete lithofacies log was created for each well and then upscaled to the 3D grid. Then, the Sequential Indicator Simulation (SIS) method was used to generate the 3D lithofacies model. Lateral continuity and vertical heterogeneity were defined by zone, and lithofacies distribution was constrained by the obtained well data. The proportion of lithofacies used to model facies distribution is shown in Table 2.

Table 2. Proportion of lithofacies by zone used for modeling facies distribution.

Formation	Lithofacies	Proportion (%)
Upper Woodford	Dolomitic Mudstone/Shale	0.0
	Chert	58.1
	Siliceous Mudstone	36.0
	Argillaceous/Siliceous Shale	5.9
Middle Woodford	Dolomitic Mudstone/Shale	0.4
	Chert	13.9
	Siliceous Mudstone	43.2
	Argillaceous/Siliceous Shale	42.5
Lower Woodford	Dolomitic Mudstone/Shale	35.0
	Chert	1.4
	Siliceous Mudstone	13.2
	Argillaceous/Siliceous Shale	50.5
Sycamore	Cherty Mudstone	27.1
	Calcareous Siltstones	73.0*
Hunton	Mud-dominated Wackestone	33.0
	Wackestone	67.0

*Though classically termed the Sycamore Limestone, recent studies have shown that some of the Sycamore is quartz silt with a calcareous matrix and contain more of a pelletal carbonate matrix (Duarte, 2018).

3.4 Petrophysical properties modeling

Petrophysical properties can be estimated from log data or measured in the laboratory from core/outcrop samples. These properties are key input parameters in reservoir characterization, production forecasting, and hydraulic fracturing treatment design. In this study, most petrophysical properties were derived from log data and reasonable estimates from published laboratory data. The Sequential Gaussian Simulation (SGS) method was used to model the properties distribution within each lithofacies and formation.

3.4.1 Porosity

Matrix porosity in the Woodford shale ranges from 0.5 to 10% with an average of 6% (Gupta et al., 2013; Ryan, 2017; Vulgamore et al., 2018), while in the Sycamore it varies from 5 to 6% (Jensen et al., 1998; Miller, 2018), and in the Hunton it ranges from 0.1 to 3% (Milad, 2019).

Commonly, a good approximation of matrix porosity is obtained from bulk density logs. Though, these values must be corrected by lithology and shale content in order to get an effective porosity.

Total and effective porosity logs were generated based on bulk density and neutron porosity data (Rider, 2000). Total porosity (ϕ_D) was calculated using Eq. 1, assuming a drilling fluid density (ρ_f) of 1 g/cm^3, and an average grain density (ρ_{ma}) of 2.61 g/cm^3 for shale (Gupta et al., 2013) and 2.71 g/cm^3 for limestone (Rider, 2000). Shale volume (V_{sh}) was estimated by Eq. 2 (Bhuyan and Passey, 1994) using 0.35 and 0.05 as reference values for neutron ($\phi_{N_{sh}}$) and density ($\phi_{D_{sh}}$) porosities of shale, respectively. Then, effective porosity (ϕ_e) was determined by Eq. 3.

$$\phi_D = \frac{\rho_{ma} - \rho_{RHOB}}{\rho_{ma} - \rho_f} \tag{1}$$

$$V_{sh} = \frac{\phi_N - \phi_D}{\phi_{N_{sh}} - \phi_{D_{sh}}} \tag{2}$$

$$\phi_e = \phi_D - \phi_{D_{sh}} * V_{sh} \tag{3}$$

Effective porosity logs were upscaled to the 3D grid using the lithofacies model as a constraint. The distribution of matrix porosity was modeled by using the SGS method, and the statistical distribution parameters shown in Table 3.

Table 3. Statistical distribution parameters used for matrix porosity modeling.

Lithofacies	Matrix Porosity			
	Min.	Max.	Mean	Std. Dev.
Argillaceous/Siliceous Shale	0.005	0.130	0.071	0.03250
Siliceous Mudstone	0.01	0.150	0.082	0.03926
Chert	0.005	0.120	0.063	0.03218
Dolomitic Mudstone/Shale	0.01	0.100	0.025	0.02830
Cherty Mudstone	0.005	0.112	0.044	0.02196
Calcareous Siltstones	0.005	0.072	0.025	0.01282
Wackestone	0.005	0.051	0.011	0.00800
Mud-dominated Wackestone	0.005	0.030	0.008	0.00783

3.4.2 Permeability

Unlike conventional reservoirs, permeability data of unconventional shale resources are usually limited or not available in the literature. Obtaining accurate measurements of permeability in shales is still a challenge. Permeability measurements can vary significantly depending on the conditions of the experiment and the type of sample that is analyzed. Though, recent publications agree that the permeability in the Woodford shale is in the range of a few hundred nanodarcy (Gupta et al., 2013; Ryan, 2017; Vulgamore et al., 2018).

The permeability model was built using the SGS method and a lognormal distribution with the statistical parameters shown in Table 4. The porosity model was used as a secondary variable constraint throughout a co-kriging coefficient. Permeabilities reported for the Sycamore (Jensen et al., 1998; Miller, 2018) and Hunton (Milad, 2019) carbonates were used to determine permeability ranges within each of these zones.

Table 4. Statistical distribution parameters used for matrix permeability modeling.

Formation	Matrix Permeability (mD)			
	Min.	Max.	Mean	Std. Dev.
Woodford	0.000001	0.001	0.0001	0.00004
Sycamore	0.0001	1	0.005	0.002
Hunton	0.01	10	0.1	0.01

3.4.3 Elastic properties

Elastic properties, such as Poisson's ratio and Young's modulus, are the most commonly used in unconventional reservoir characterization since they can be used to define the brittleness or ductility of a rock. These properties usually exhibit a significant variation between formations and within the Woodford shale interval. This variation depends mainly on the mineralogy composition and the rock fabric (Abouelresh and Slatt, 2011; Sierra et al., 2010; Slatt, 2013). Understanding the distribution and relationship of these mechanical properties is key to drilling, fracturing, and production of any shale play.

These properties can be derived from sonic logs or laboratory measurements. In this study, compression and shear wave velocities and density logs provided most of the information to determine the mechanical rock properties. Compressional wave velocity (V_p) was derived from DTC logs (Eq. 4). Shear wave velocity (V_s) was estimated from V_p using the empirical relationship shown in Eq. 5 (Castagna et al., 1985) since DST logs were not available. Eq. 6 to 9 were used to calculate Poisson's ratio (ν), Young's modulus (E), shear modulus (K), and bulk modulus (G).

$$V_p = 10^6/DTC \tag{4}$$

$$V_p = 1.16V_s + 1.36 \tag{5}$$

$$\nu = \frac{V_P^2 - 2V_s^2}{2(V_P^2 - V_s^2)} \tag{6}$$

$$E = \frac{\rho_{RHOB} V_s^2 (3V_P^2 - 4V_s^2)}{(V_P^2 - V_s^2)} \tag{7}$$

$$K = \rho_{RHOB} V_p^2 - \frac{4}{3}\rho_{RHOB} V_s^2 \tag{8}$$

$$G = \rho_{RHOB} V_s^2 \tag{9}$$

Similar to porosity modeling, mechanical property logs were upscaled to the 3D grid using the lithofacies model as a constraint. 3D models were built by using SGS and the normally distributed parameters obtained from the corresponding upscaled logs.

3.5 Results

As mentioned previously, lithofacies were classified and correlated with outcrop and core interpretations to build a representative 3D lithofacies model of the study area. Figure 9 presents an east-west sectional view of the lithofacies model. In general, the lateral continuity and vertical heterogeneity of the Woodford within the study area is preserved and supports observations made by different authors (Becerra, 2017; Brito, 2019; Galvis-Portilla, 2017; Higley et al., 2018; Lambert, 1993; Sierra et al., 2010; Slatt, 2013).

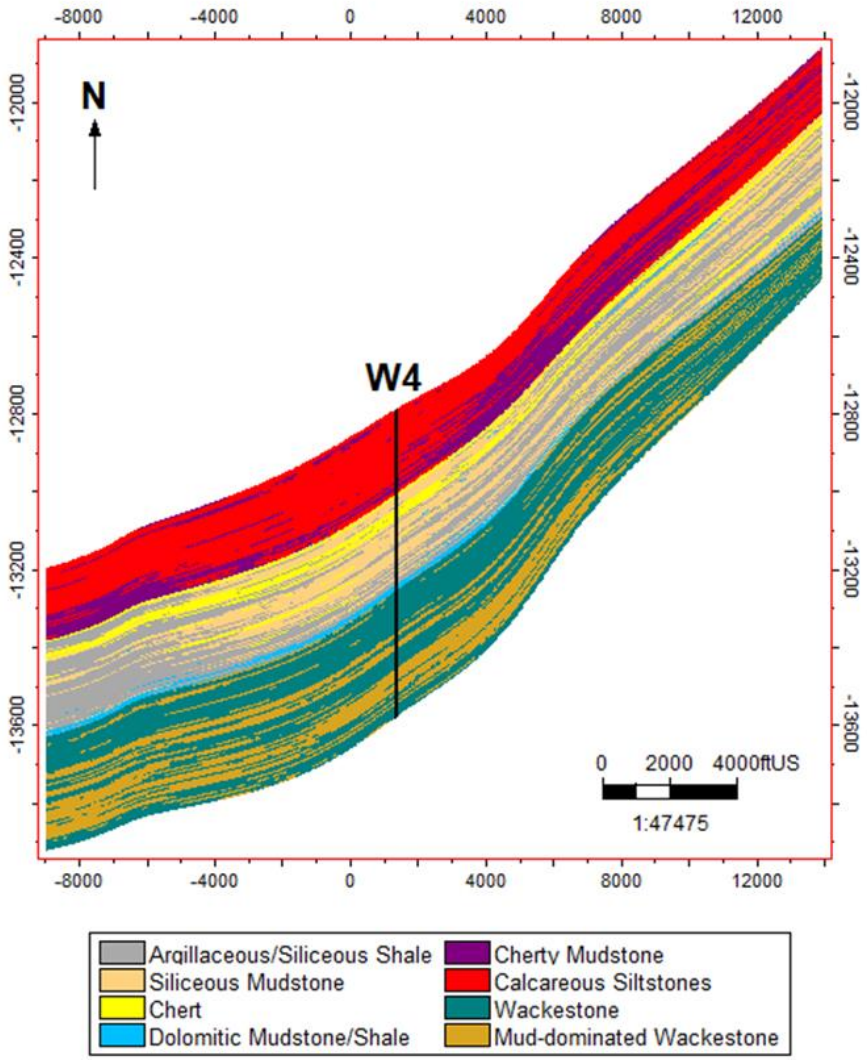

Figure 9. East-west sectional view of the 3D lithofacies model.

The lower Woodford contains the most clay-rich lithofacies, with the Argillaceous, Siliceous, and Dolomitic shales being the most abundant (Figure 10). The most quartz-rich lithofacies are within the upper zone, represented by more than 90% of Cherts and Siliceous Mudstones. The middle Woodford contains mostly Argillaceous/Siliceous Shales, Siliceous Mudstones and Cherts. Generally, among the three Woodford members, clay-rich lithofacies decreases upward, while quartz-rich lithofacies increases upward.

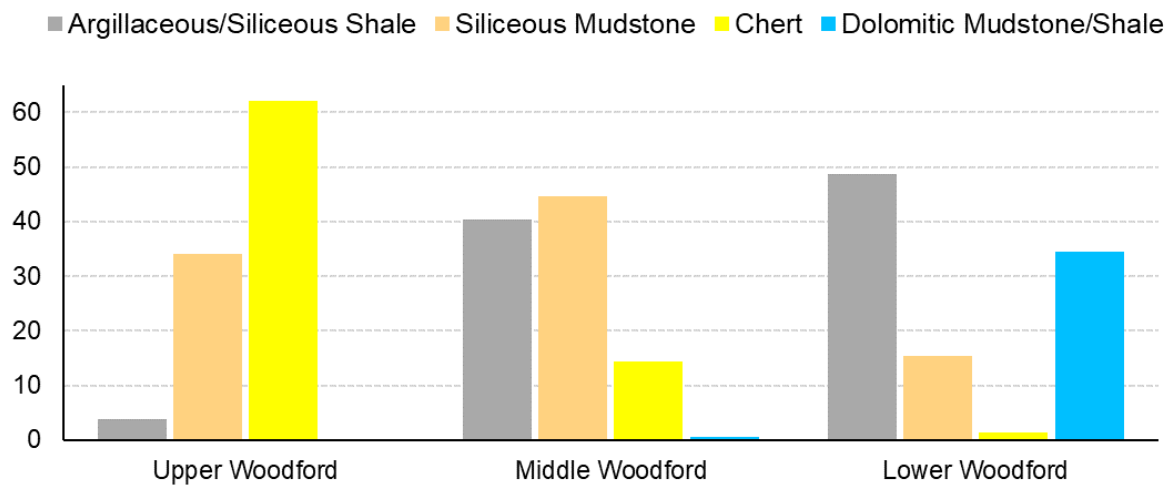

Figure 10. Distribution of lithofacies within the Woodford zone in the 3D model.

Some of the petrophysical property models are shown in Figure 11. A significant contrast is observed among each of the three formations and within the Woodford interval. The Sycamore and Hunton exhibit low porosity, and high permeability, which is typical of some carbonates. Calcite cementation tends to reduce porosity, while interconnected fractures and vugs tend to increase the permeability. Porosity and permeability within the Woodford average 7% and 100 nanodarcy, as expected.

An important distinction is also noticed with the Poisson's ratio and Young's modulus distribution models. These two properties measure the amount of strain and deformation experienced by a rock when stress is applied. Rocks with relatively large Poisson's ratio and small Young's modulus are considered as ductile rocks. These types of rocks exhibit a plastic deformation before breakage, which means it is more difficult to fracture them. Rocks with high clay content usually present a ductile behavior. Alternatively, relatively low values of Poisson's ratio and high values of Young's modulus are characteristic of brittle rocks. Brittle rocks tend to

break without prior plastic deformation. Quartz- and dolomite-rich rocks usually exhibit brittle behavior (Slatt, 2011).

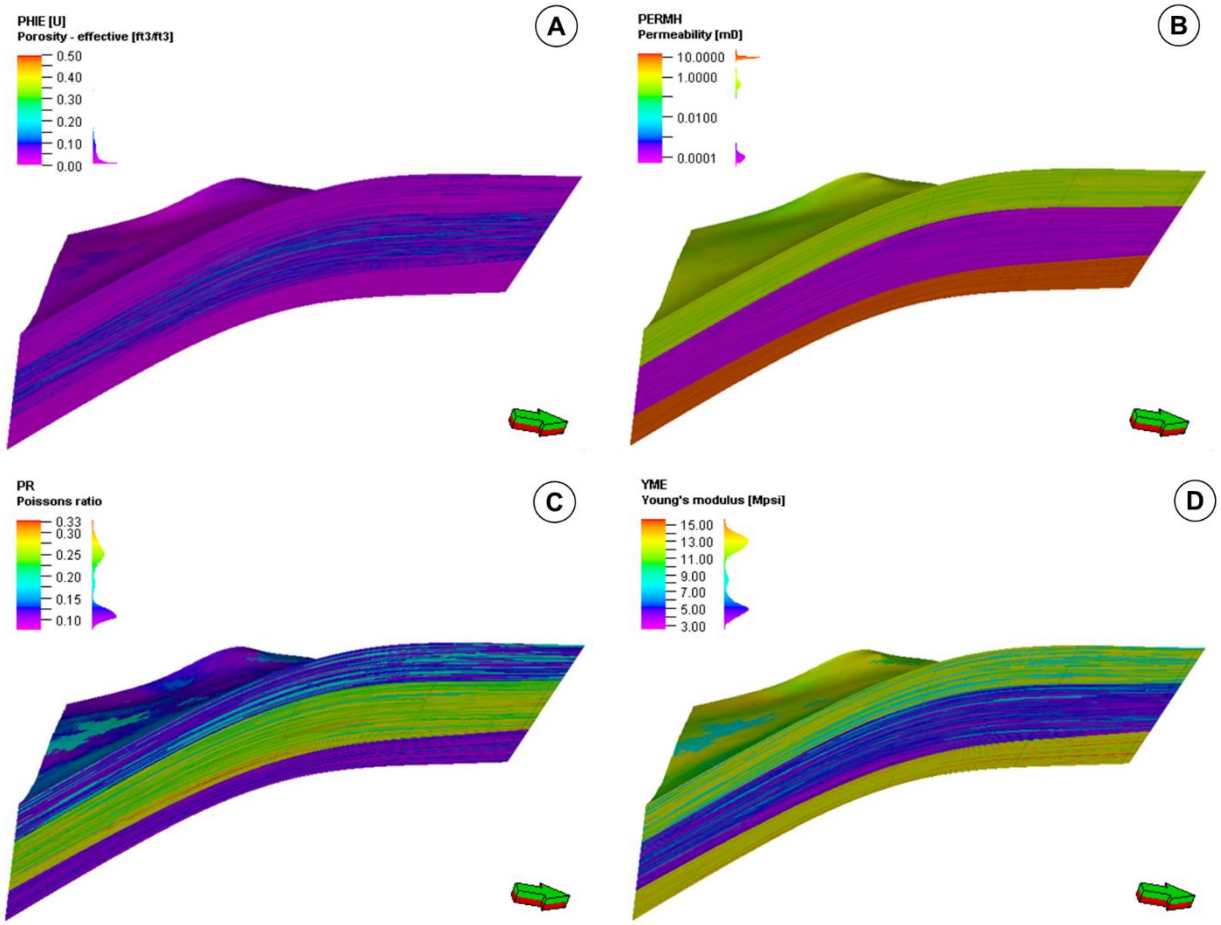

Figure 11. Petrophysical property models. (A) Porosity, (B) permeability, (C) Poisson's ratio, and (D) Young's modulus.

A cross plot of Poisson's ratio against Young's modulus colored by lithofacies is presented in Figure 12. This relationship illustrates that both the Sycamore and Hunton formations are more brittle than the Woodford. It also explains that within the Woodford, quartz-rich lithofacies (cherts and siliceous mudstones) will be more prone to fracture, compared to clay-rich lithofacies, due to their relative brittleness.

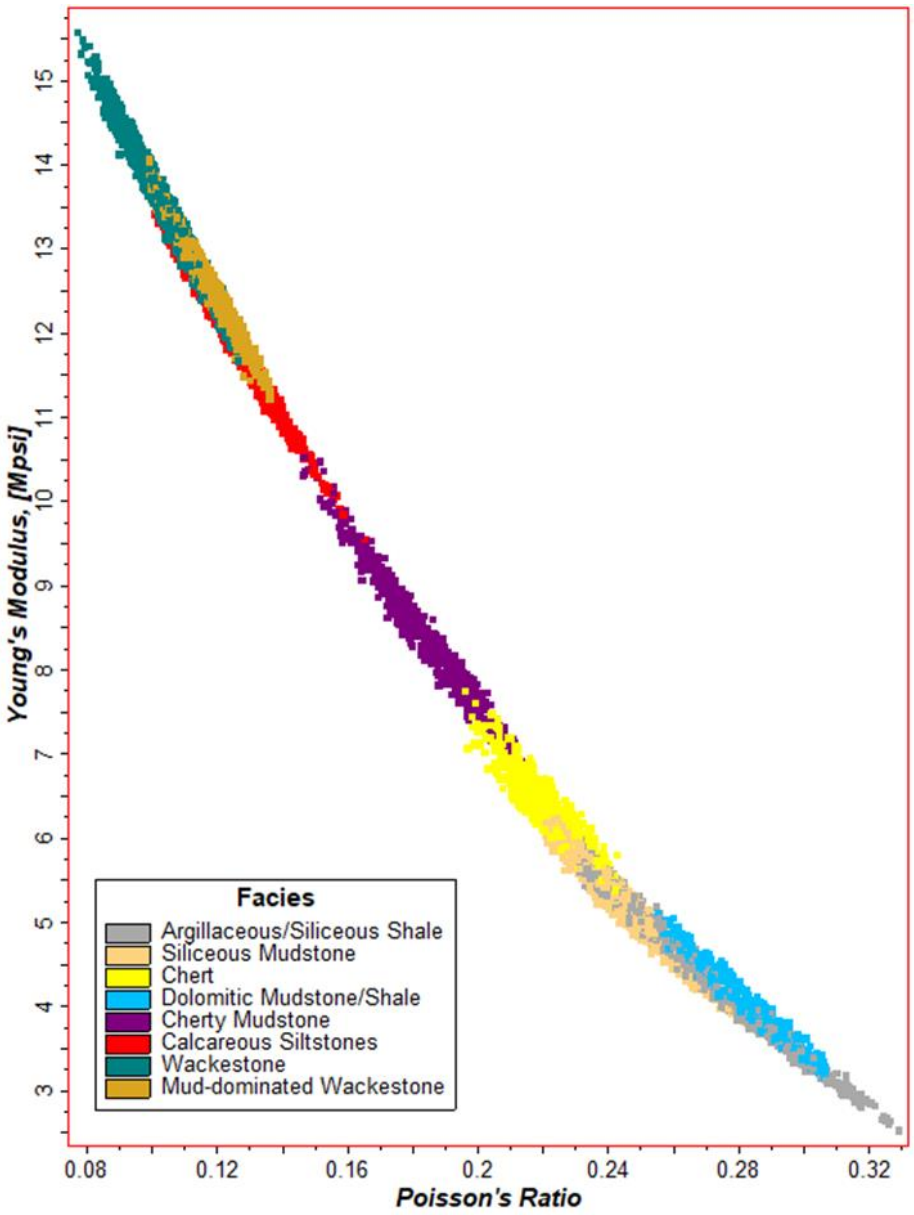

Figure 12. Cross plot of Poisson's ratio vs. Young's Modulus colored by lithofacies.

Chapter 4: Hydraulic Fracture Modeling

This chapter discusses the methodology and data used to model the hydraulic fracture growth and propagation on a single horizontal well in the Woodford Shale. The purpose is to integrate the geological model presented in Chapter 3 within GOHFER®, a commercial 3D fracture modeling software program, to evaluate the size and characteristics of the resulting stimulated reservoir volume (SRV). Results are presented at the end of the chapter. Hydraulic fracturing model will be used later for dynamic flow simulation.

4.1 3D Geomechanical earth model

Geomechanical earth models integrate in-situ stress information and mechanical rock properties, which form the basis for hydraulic fracture modeling. Properties such as porosity, permeability, bulk density, Poisson's ratio, and Young's modulus (obtained from the geological model introduced in Chapter 3) were used here as input for the geomechanical earth model setup.

The in-situ minimum horizontal stress (S_{hmin}) profile against depth (D_{tv}) is automatically calculated from pore pressure gradient (γ_p), overburden gradient (γ_{ob}), Poisson's ratio (ν), Young's modulus (E), Biot's constants (α_v, α_h), tectonic strain (ε_x), and tectonic stress (σ_t) as shown in Eq. 10 (Barree and Associates LLC, 2017).

$$S_{hmin} = \frac{\nu}{(1-\nu)}\left[D_{tv}\gamma_{ob} - \alpha_v\left(D_{tv}\gamma_p\right)\right] + \alpha_h\left(D_{tv}\gamma_p\right) + \varepsilon_x E + \sigma_t \quad (10)$$

Tectonic forces were assumed to be negligible since no information was available, and the area is currently considered to be relaxed tectonically. Overburden gradient was set to 1 psi/ft, and default values of Biot's constants were preserved. Two pore pressure gradients, 0.44 and 0.65 psi/ft, were considered in this study due to the pressure variations reported in the Anadarko Basin

(McKeon, 2011; Nelson and Gianoutsos, 2014). The stress anisotropy (i.e., the difference between the minimum and maximum horizontal stress) was estimated by the software from log porosity data.

Unlike the geological model, the geomechanical earth model encompasses a smaller area of 1.33 x 0.95 miles (2.1 x 1.5 km). A 4,000 ft long lateral well was located within this area (Figure 13) to simulate a multi-stage hydraulic fracture treatment. A reference well was also located at the center of the grid. The treatment well was oriented north-south, perpendicular to the current maximum horizontal stress (S_{Hmax}), which azimuth is about N85E ±5 (Ghosh, 2017; Jing Zhang, 2016; Molinares-Blanco et al., 2017). The lateral of the well was placed within the upper section of the middle Woodford, which has been identified as the preferred target zone due to the presence of about 50% each of alternating thinner brittle beds and TOC-rich more ductile beds (Brito, 2019; Galvis-Portilla, 2017; Sierra et al., 2010; Slatt, 2013). Figure 14 depicts a longitudinal view of the well within the Woodford interval along with the calculated total stress (S_{hmin}) for Case A1 (presented in the next section) as background.

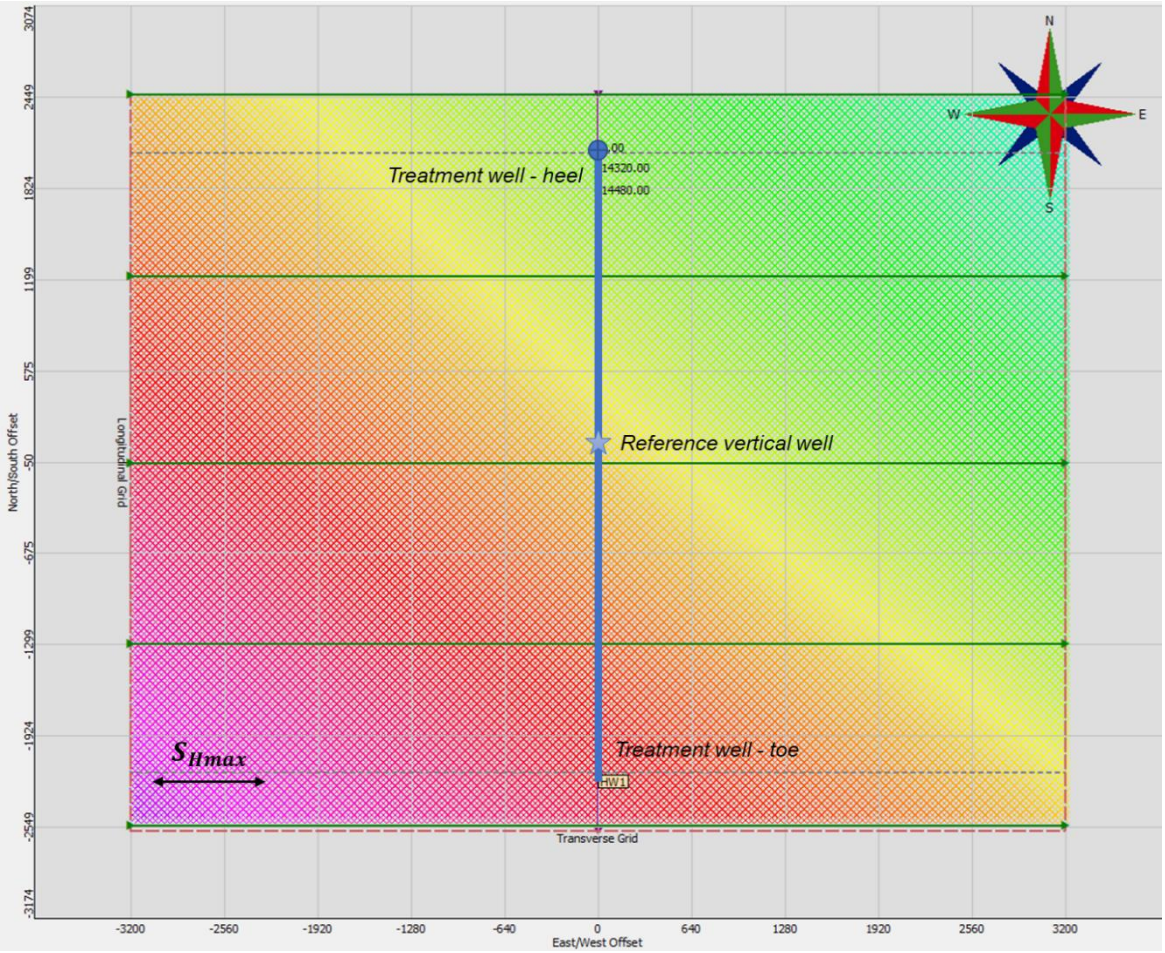

Figure 13. Map view of the well location within the geomechanical model. The treatment well is oriented north-south, perpendicular to the current maximum horizontal stress, and the vertical reference well is located at the center of the grid.

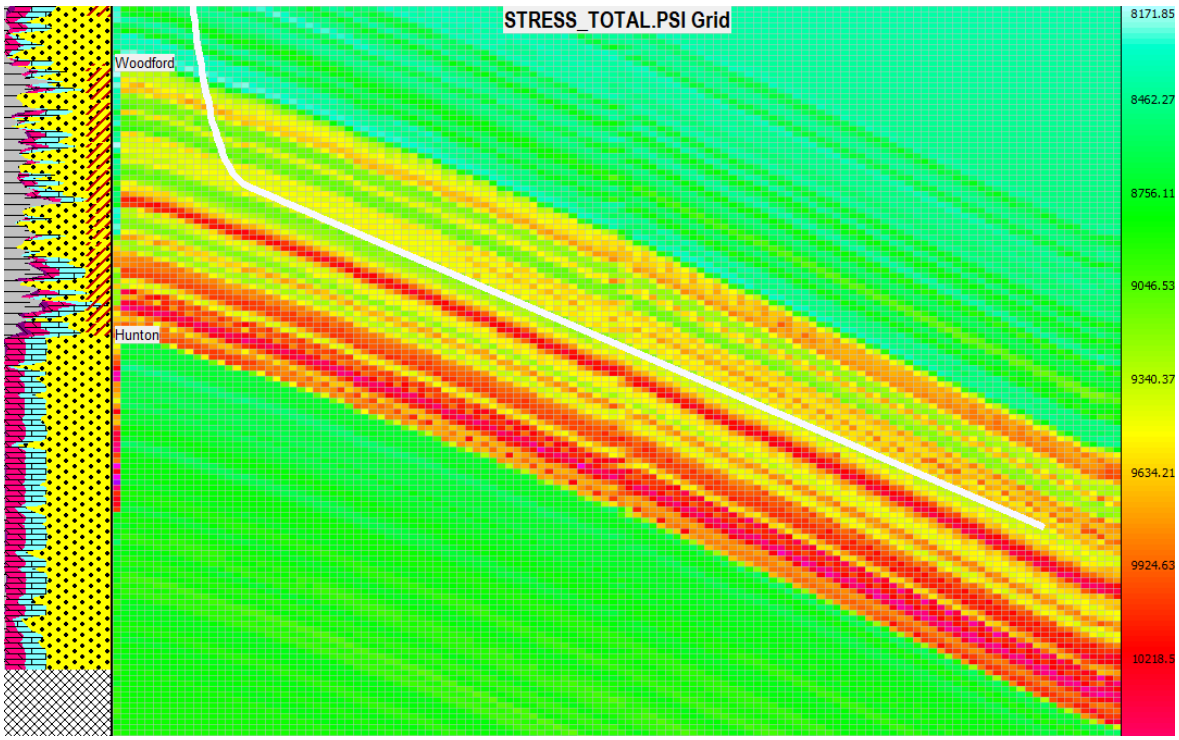

Figure 14. Longitudinal view of the well location within the Woodford interval. Calculated total stress grid for a pore pressure gradient of 0.44 psi/ft (Case A1) is in the background, and a lithology log is on the left.

4.2 Hydraulic fracture treatment design

The stimulation treatment design on the 4,000 ft lateral included eight stages with four clusters per stage. The 2 ft long clusters were evenly spaced every 100 ft. Each stage consisted of 20,133 barrels (615,000 gallons) of slickwater and 649,500 pounds of proppant. In order to understand the complexity of the fracture network generated within the Woodford, eight fracturing designs were outlined, as shown in Table 5. Two pressure gradients were assumed to illustrate the variations in pore pressure mentioned earlier. Curable resin-coated (CRC) sand and ceramic proppant (Bauxite) were used as proppant agents to evaluate the impact of high closure stress on the proppant pack. Pressure-dependent leakoff (PDL) coefficient was included to account for the

additional leakoff generated by the opening of natural fractures (Barree and Associates LLC, 2017).

Table 5. Design parameters for each fracturing treatment.

Case	Pore pressure gradient (psi/ft)	PDL coefficient (1/psi)	Proppant type	Proppant proportion (%)
A1	0.44	0.0002	40/70 CRC Sand 20/40 CRC Sand	10 90
A2		0.001		
A3		0.002		
A4		0.0002	40/70 CRC Sand 20/40 Bauxite	35 65
B1	0.65	0.0002	40/70 CRC Sand 20/40 CRC Sand	10 90
B2		0.001		
B3		0.002		
B4		0.0002	40/70 CRC Sand 20/40 Bauxite	35 65

Table 6 shows the pumping schedule per each stage that was used for all the treatment designs. Figure 15 depicts an example of the resulting treatment plot for fracturing design A1, Stage #8. For the sake of simplicity, only transverse fractures were modeled. Also, stress shadowing between clusters was considered, but not between stages.

Table 6. Pumping schedule per stage used for each stimulation treatment design.

Elapsed time (minutes)	Clean Stage Volume (gal)	Proppant Concentration (lbm/gal)	Slurry Rate (bbl/min)
21.18	80,000	0	90
26.51	20,000	0.1	90
34.53	30,000	0.25	90
45.36	40,000	0.5	90
56.32	40,000	0.75	90
75.69	70,000	1	90
98.04	80,000	1.25	90
120.68	80,000	1.5	90
143.53	80,000	1.75	90
166.6	80,000	2	90
170.56	15,000	0	90

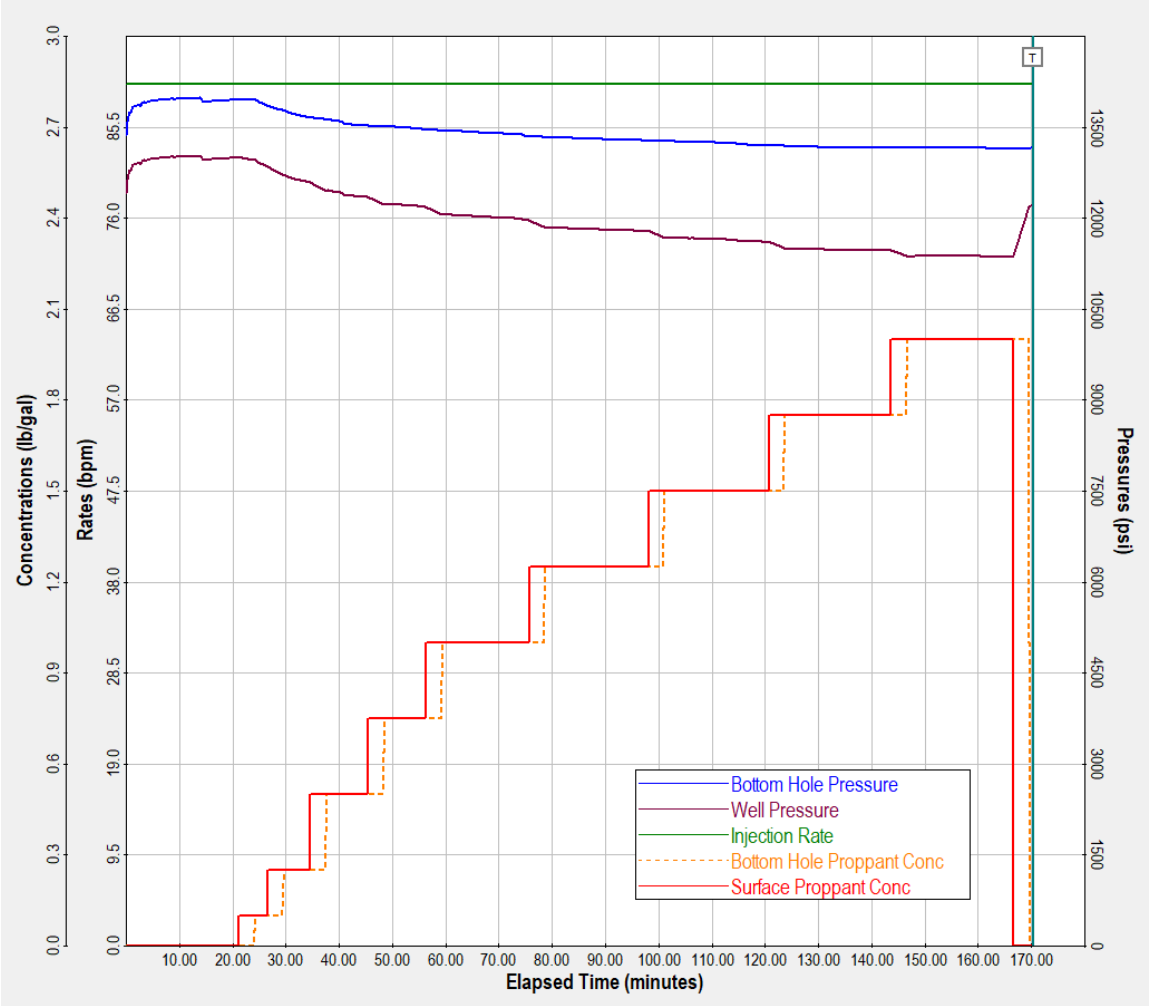

Figure 15. Fracturing treatment plot for Case A1, Stage #8.

4.3 Results

Table 7 shows a summary of the simulation results. For each case, the average gross and propped fracture half-length is specified, along with their corresponding average fracture height, width, and proppant concentration. The stimulated reservoir volume (SRV) was also determined based on the average fracture half-length, fracture height, and cluster size assuming an ellipsoidal shape. Results are listed in Table 8.

Table 7. Average fracture half-length, height, width, and proppant concentration for each treatment design case.

Case	Average Gross Fracture Half-Length (ft)	Average Propped Fracture Half-Length (ft)	Average Fracture Height (ft)	Average Proppant Concentration (lb/ft²)	Average Fracture Width (in)
A1	3240	368.8	87.7	0.279	0.196
A2	3240	258.8	55.2	0.299	0.197
A3	3240	261.3	38.6	0.321	0.197
A4	3240	703.8	87.3	0.361	0.192
B1	3240	207.5	145.2	0.210	0.172
B2	3240	210.0	85.6	0.276	0.178
B3	3240	198.8	46.1	0.305	0.187
B4	3240	482.5	153.1	0.275	0.169

Table 8. Gross and effective stimulated reservoir volume (SRV) for each case.

Case	Gross SRV (ft3)	Effective SRV (ft3)
A1	1.52E+08	1.73E+07
A2	9.58E+07	7.65E+06
A3	6.70E+07	5.41E+06
A4	1.52E+08	3.30E+07
B1	2.52E+08	1.61E+07
B2	1.49E+08	9.64E+06
B3	8.01E+07	4.91E+06
B4	2.66E+08	3.96E+07

In general, it was found that fracture characteristics change significantly from one case to another. Although the purpose of this study was not to find the optimum fracturing design, the effect of some design parameters will be discussed in the next sections.

4.3.1 Pore pressure, total stress and their effect on fracture geometry

The creation and propagation of fractures are controlled by the magnitude and direction of the minimum horizontal stress. Initially, fractures propagate perpendicular to the minimum horizontal stress, then the stress differences between formations control whether the fracture grows

upward or downward. As observed in Figure 16a, lower pore pressure gradient translates into lower total stress, and therefore, larger fractures are created (Figure 16b). These larger fractures are usually contained within the Woodford and display less fracture height (Figure 16c). On the other hand, cases with a higher pore pressure gradient exhibit shorter fractures that grow much more vertically, even beyond the Woodford interval (Figure 17). This upward growth occurs because the stress tends to decrease above the landing zone (higher proportion of brittle intervals) and increase below (higher proportion of ductile intervals). Similar upward fracture growth has been observed when analyzing microseismic data from Woodford wells (Hai et al., 2017; Jing Zhang, 2016; Molinares-Blanco et al., 2017).

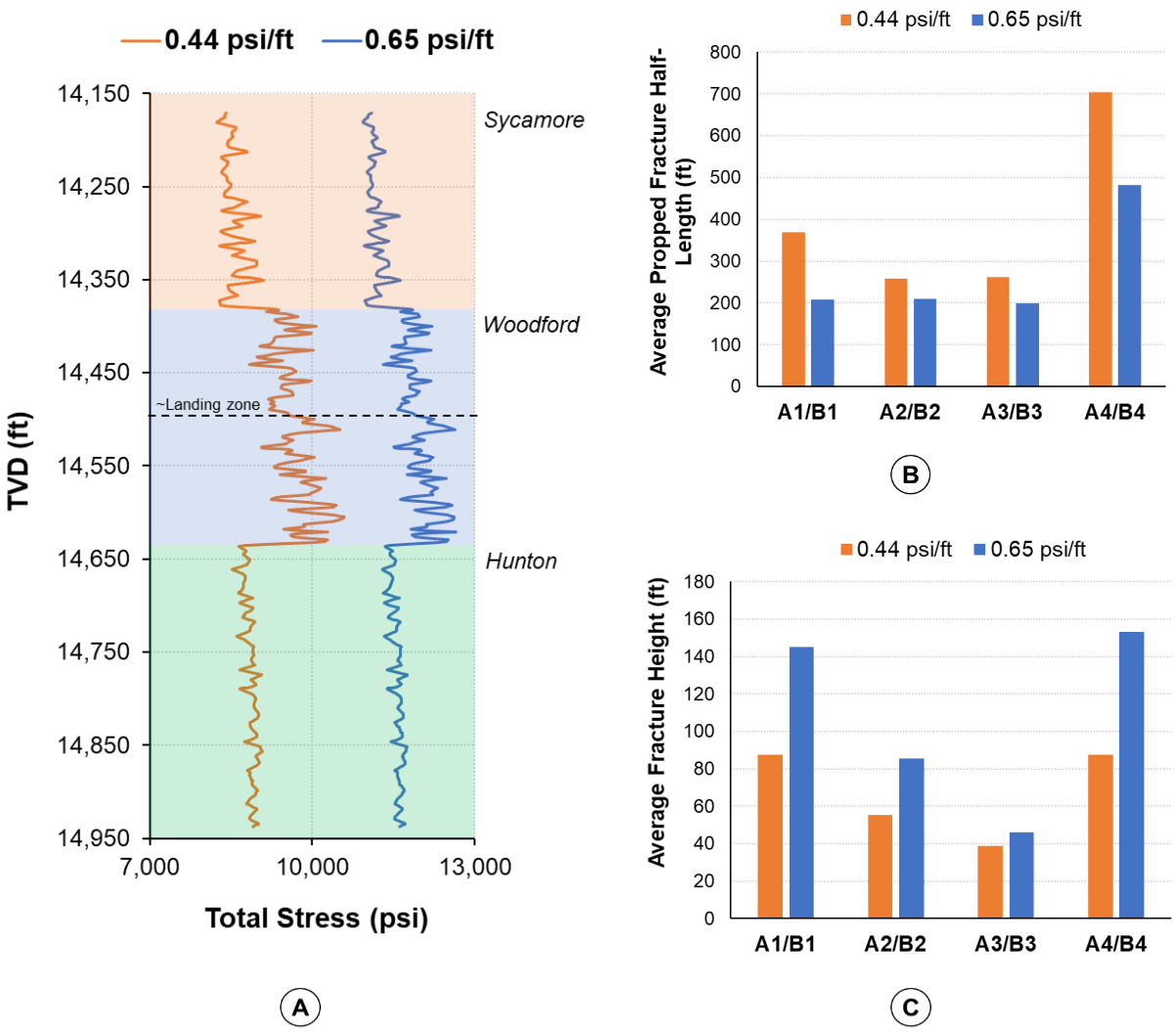

Figure 16. Pore pressure gradient comparison. (A) Stress profile on the reference well location, (B) average propped fracture half-length, and (C) average fracture height for each simulated case.

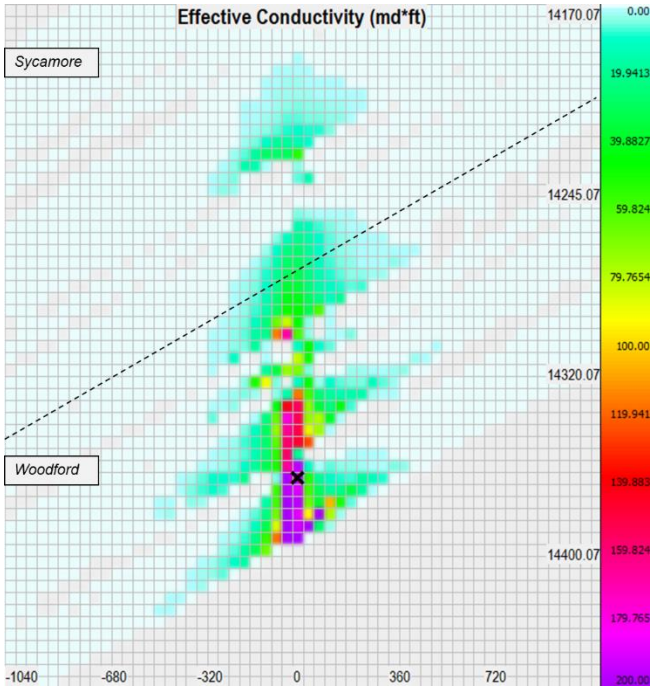

Figure 17. Example of upward fracture growth beyond the Woodford shale. Effective conductivity of Transverse Fracture 4, Stage 8, Case A4.

4.3.2 Pressure-dependent leakoff (PDL) and its effect on fracture geometry

The pressure-dependent leakoff estimates the amount of fracturing fluid that is lost due to the opening of pre-existing natural fractures (Figure 18). As the induced hydraulic fractures propagate, the fracturing pressure increases and reaches the maximum horizontal stress, also known as the critical fissure opening pressure. This causes natural fractures to dilate, increasing the fluid leakoff, and resulting in shorter fractures. Figure 19 depicts a comparison between three different values of PDL coefficient and its effect on fluid loss and fracture geometry. As shown in Figure 19a, higher PDL coefficients lead to higher leakoff and therefore, smaller SRVs (Figure 19b), regardless of the pore pressure gradient.

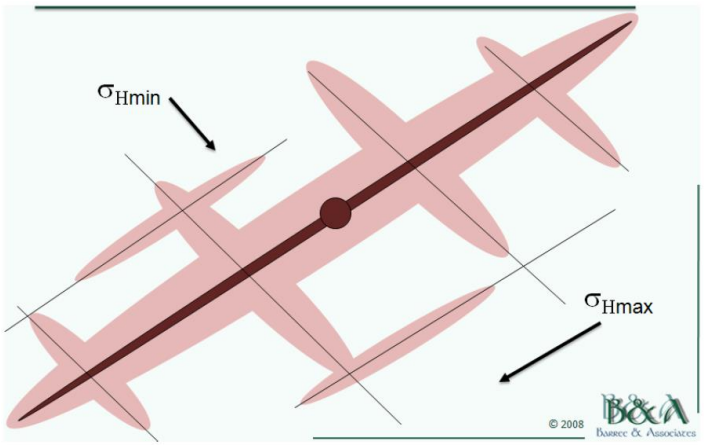

Figure 18. Conceptual model of pressure-dependent leakoff due to the presence of natural fractures parallel to the maximum horizontal stress (from (Barree and Associates LLC, 2017))

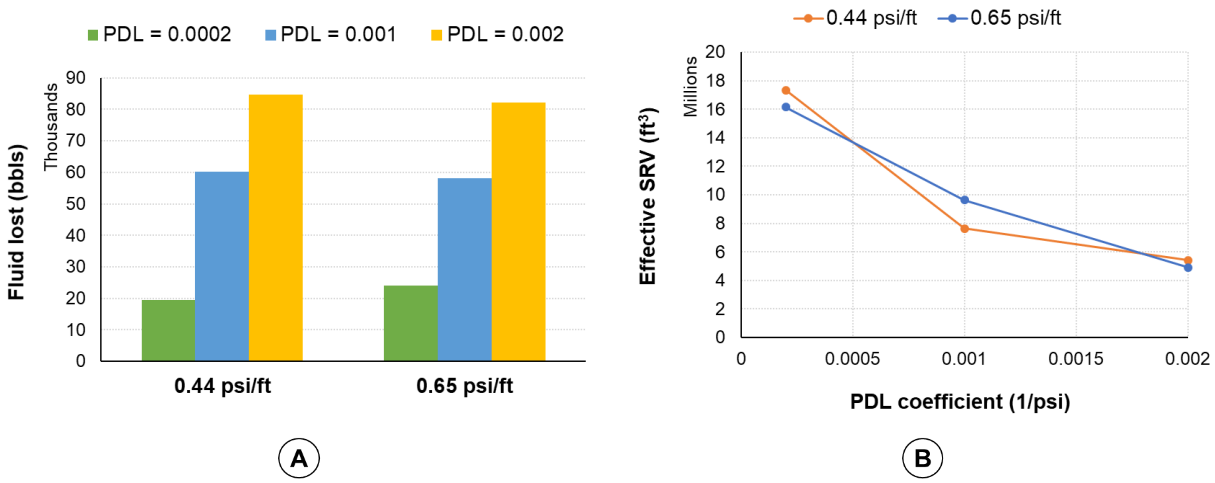

Figure 19. PDL coefficient comparison. (A) Total fluid lost (leakoff) for different PDL coefficients. (B) Effective stimulated reservoir volume vs. PDL coefficient.

4.3.3 Proppant type, total stress, and their effect on fracture conductivity

Due to the depth and high closure stress in Anadarko Basin wells, the most commonly used proppant types are curable resin-coated sand and ceramic proppant (Grieser, 2011). These types of proppants improve proppant pack strength and conductivity, lessening the generation and

migration of proppant fines, and preventing detrimental proppant flowback (Hu et al., 2015; Terracina, 2011). Figure 20 shows the maximum fracture conductivity that was obtained for the two types of proppant used at the two-pore pressure gradients that were assumed. As illustrated, more crush-resistant proppant, such as bauxite (a ceramic proppant), results in higher fracture conductivity when compared to curable resin-coated sand.

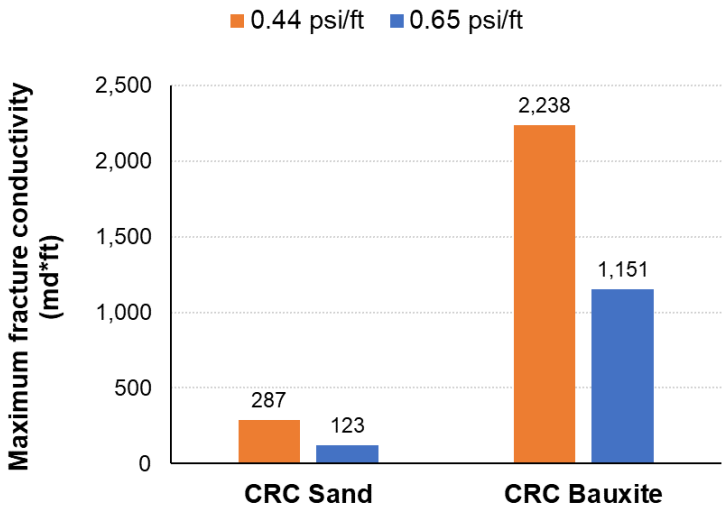

Figure 20. Maximum fracture conductivity for CRC sand and CRC bauxite at two different pore pressure gradients.

A decline in the conductivity is also noted in Figure 20, with an increase in total stress (or pore pressure gradient). High closure stress reduces porosity and width of the proppant pack, which usually lead to fines generation and loss of conductivity. However, stress is not the only factor that controls the final fracture conductivity. Factors such as proppant concentration and grain size also have a significant impact on conductivity (Barree, 2016).

Chapter 5: Numerical Reservoir Simulation

In this chapter, the methodology and data used to perform integrated reservoir simulation are discussed. The purpose is to combine the geological model presented in Chapter 3 with the resulting hydraulic fracture set given in Chapter 4 to evaluate the well production performance using ECLIPSE™, a commercial numerical reservoir simulator. Results are presented at the end of the chapter.

5.1 Simulation model setup

5.1.1 Dual porosity model

Dual porosity models are usually used in unconventional reservoir simulation. Due to the high contrast between fracture and matrix permeabilities, it is assumed that the volume of hydrocarbon is stored in both matrix and fractures, but flow occurs mainly within the fractures. In this study, the petrophysical model introduced in Chapter 3 served as the matrix property model on the dual porosity model. The 3D grid used for flow simulation comprises only a sector of the original geological model with an area of 1.33 x 0.95 miles (2.1 x 1.5 km), and 175x125x175 cells. Fracture network properties were defined for both natural and hydraulically induced fractures. Preliminary porosity and permeability models for the fracture network were generated by SGS using the statistical distribution parameters shown in Table 9 and Table 10.

Table 9. Statistical distribution parameters for the network porosity model.

Formation	**Fracture Porosity**			
	Min.	Max.	Mean	Std. Dev.
Woodford	0.000395	0.00615	0.001828	0.001028
Sycamore	0.000265	0.00979	0.001998	0.000749
Hunton	0.000325	0.00976	0.001999	0.007496

Table 10. Statistical distribution parameters for the network permeability model.

Formation	Fracture Permeability (mD)			
	Min.	Max.	Mean	Std. Dev.
Woodford	0.01	149.99	1.415	6.4237
Sycamore	0.01	99.24	0.697	2.1962
Hunton	0.01	198.10	0.772	2.1357

Induced fractures were modeled through transmissibility (permeability) multipliers. Figure 21 illustrates the transmissibility multiplier that describes the geometry and conductivity of B1's induced fracture network, presented in Chapter 4. Matrix-fracture interaction was set up to be higher within the SRV (near the wellbore) and much lower away from the wellbore. Figure 22 shows a lateral view of the resulting transmissibility factor of the fracture network model along the well trajectory for case B1.

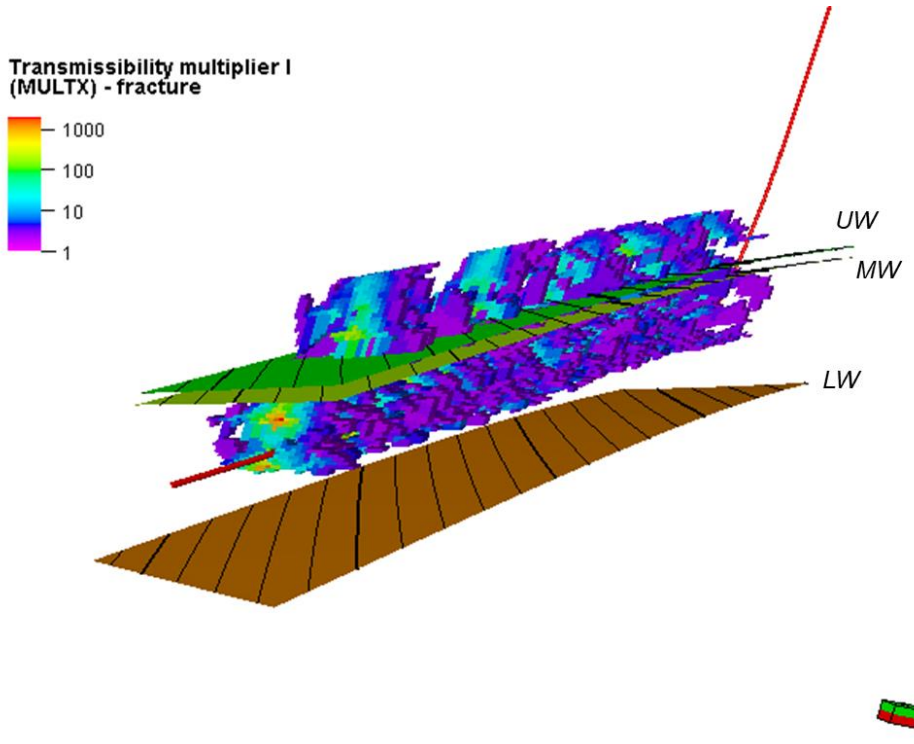

Figure 21. Transmissibility multipliers used to describe hydraulic fracture geometry and conductivity (Case B1).

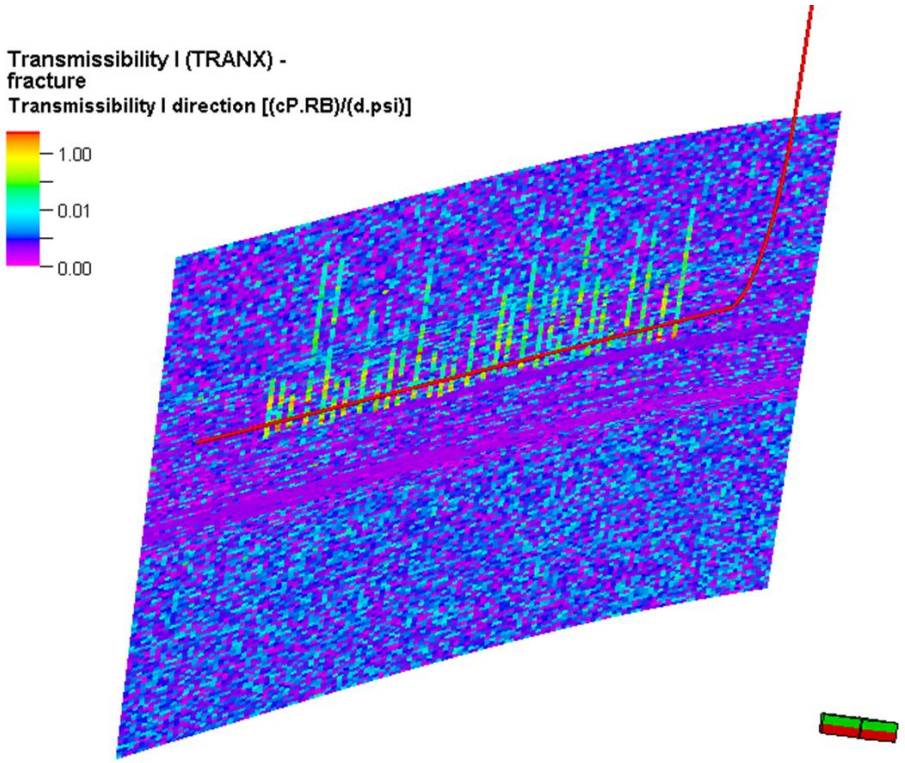

Figure 22. Side view of the resulting transmissibility factor of the fracture network model in X-direction – Case B1.

5.1.2 Initial reservoir pressure and fluid saturations

Reservoir fluid was modeled as black oil with the properties shown in Table 11. The initial reservoir pressure for both the matrix and fracture model was assumed to be the same, and it was calculated using an average pressure gradient of either 0.44 psi/ft or 0.65 psi/ft in order to match the analysis performed in Chapter 4. Figure 23 depicts a side view of the matrix pressure profile along the well trajectory. Initial fluid saturation distributions were assumed to the same for both the matrix and fracture model. Connate water saturation for each formation was estimated by J-functions (Gonzalez, Perozo, and Medina, 2016; Phelps, 1993), obtaining an average of 28% for the Sycamore (Clark and Wall, 2007), 40% for the Woodford (Hai et al., 2017), and 54% for the Hunton (M. Gupta, Joshi, and Kelkar, 2005). No initial free gas was assumed.

Table 11. Reservoir fluid properties used for flow simulation

Oil API gravity	40
Solution GOR (Mscf/stb)	0.8476
Gas specific gravity	0.8
Water salinity (ppm)	70,000
Reservoir temperature (°F)	230

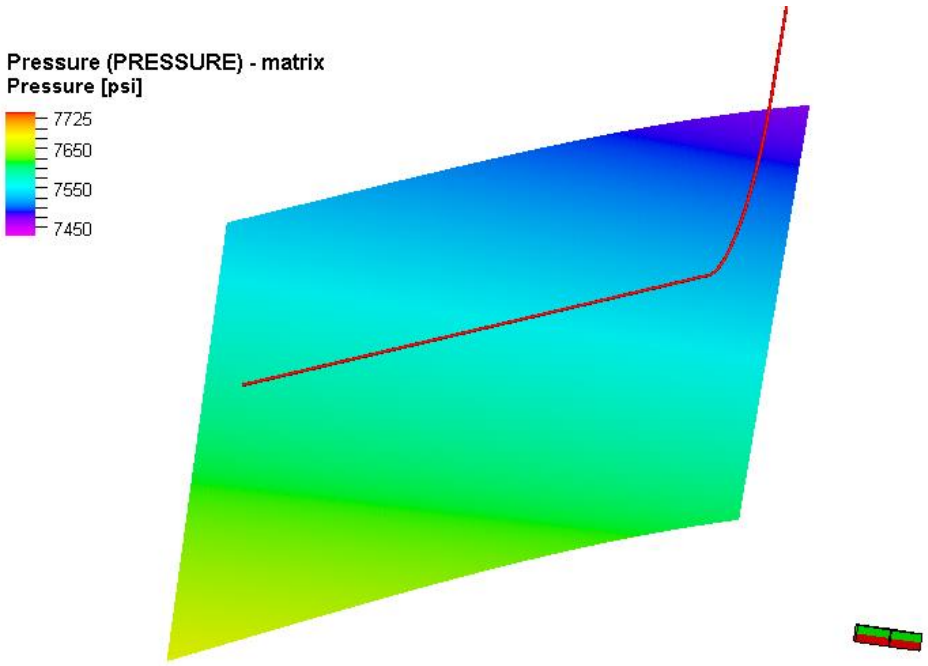

Figure 23. Side view of the matrix-pressure profile along the well trajectory – Case B1.

5.1.3 Rock compaction tables

Rock compaction tables were included to account for changes in porosity and permeability with pressure. Table 12 shows an example of the original multipliers used for hydraulic fractures in Case B1. Since no rock compaction data for the Woodford Shale was available, these multipliers were adjusted later on during the simulation.

Table 12. Rock compaction tables for hydraulic fractures (Case B1).

Pressure (psi)	Multipliers			
	Porosity	x-Transmissibility	y-Transmissibility	z-Transmissibility
500	0.30	0.247	0.247	0.247
2,000	0.45	0.333	0.333	0.333
4,000	0.65	0.497	0.497	0.497
6,000	0.85	0.741	0.741	0.741
7,500	1.00	1.000	1.000	1.000
9,000	1.15	4.480	1.820	1.560
11,000	1.35	33.11	4.050	2.850
13,000	1.55	244.7	9.020	5.200
15,000	1.75	1,808	20.08	9.480

5.2 Results

In an attempt to account for the amount of water injected into the formation during the stimulation treatment, a water injection phase was simulated prior to the production phase. Figure 24 shows the oil/gas/water distribution around the wellbore at the end of the injection phase for Case B1. Injected water flows mainly through the hydraulic fractures. According to the stimulation treatment design, about 117,000 barrels of water are injected in total. Though, after many efforts, no more than half of the total water was possible to inject (Figure 25) with the simulation. The same occurred for all the cases.

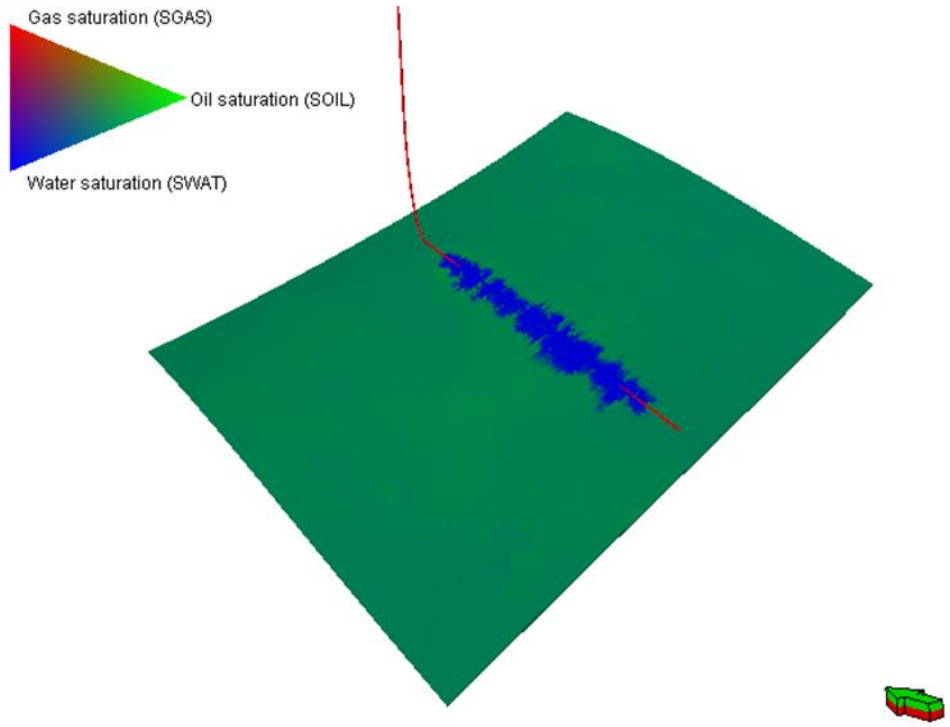

Figure 24. Fracture saturation profile at the end of the water injection phase (Case B1).

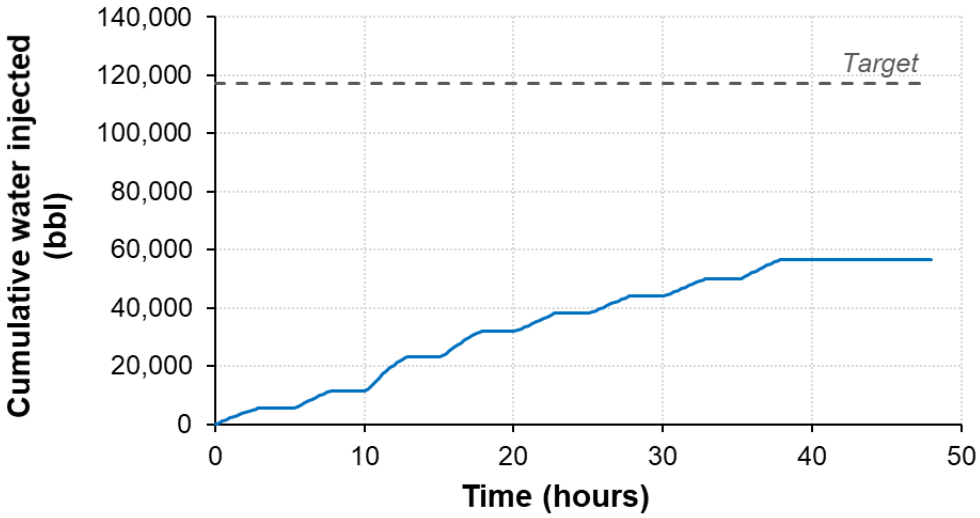

Figure 25. Cumulative water injected at the end of the injection phase (Case B1).

Well production performance was evaluated for two years with a target liquid rate of 1,000 BPD and a bottom hole pressure (BHP) limit of 500 psi. Figure 26 and Figure 27 show the two-years forecasted oil rate, bottom hole pressure, water cut, and gas-oil ratio for Case B1. Notice the well immediately reaches the BHP limit, water cut drops below 5% within the first year of production, and gas-oil ratio (GOR) remains the same. Oil rate increases with time and reaches its maximum within the first 250 days of production, and then, it declines very slowly. The fracture pressure drop is also very small, only about 200-300 psi, at the end of the production period, as illustrated in Figure 28.

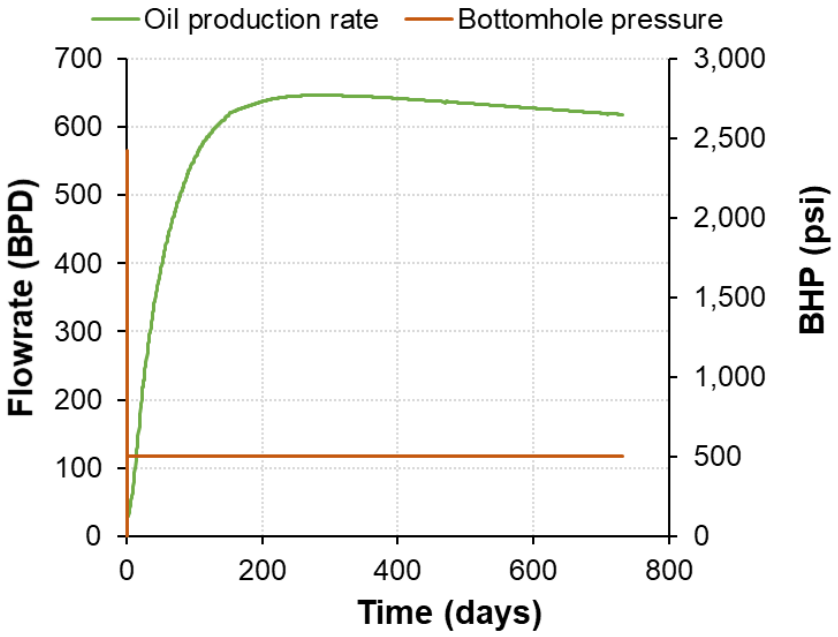

Figure 26. Predicted oil rate and bottom hole pressure (Case B1).

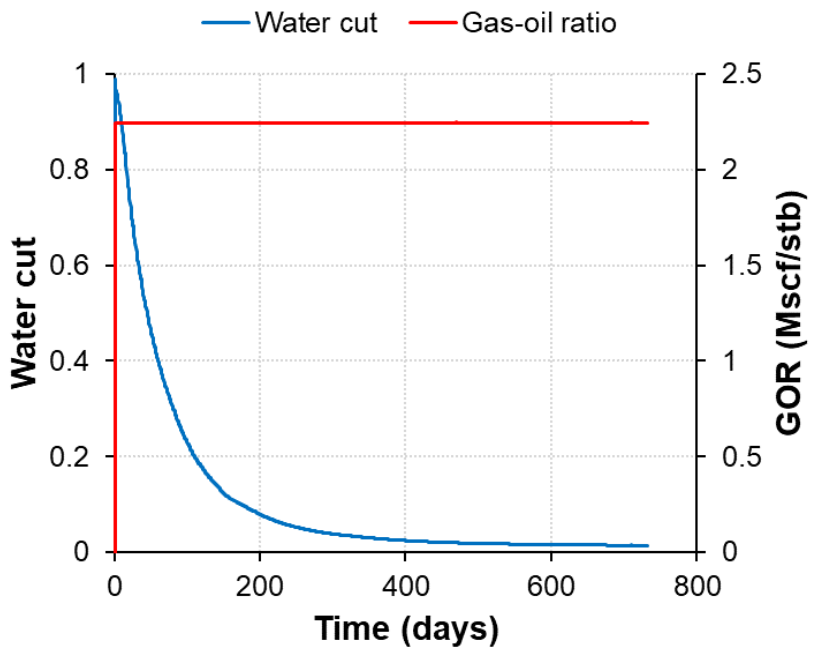

Figure 27. Predicted water cut and gas-oil ratio (Case B1).

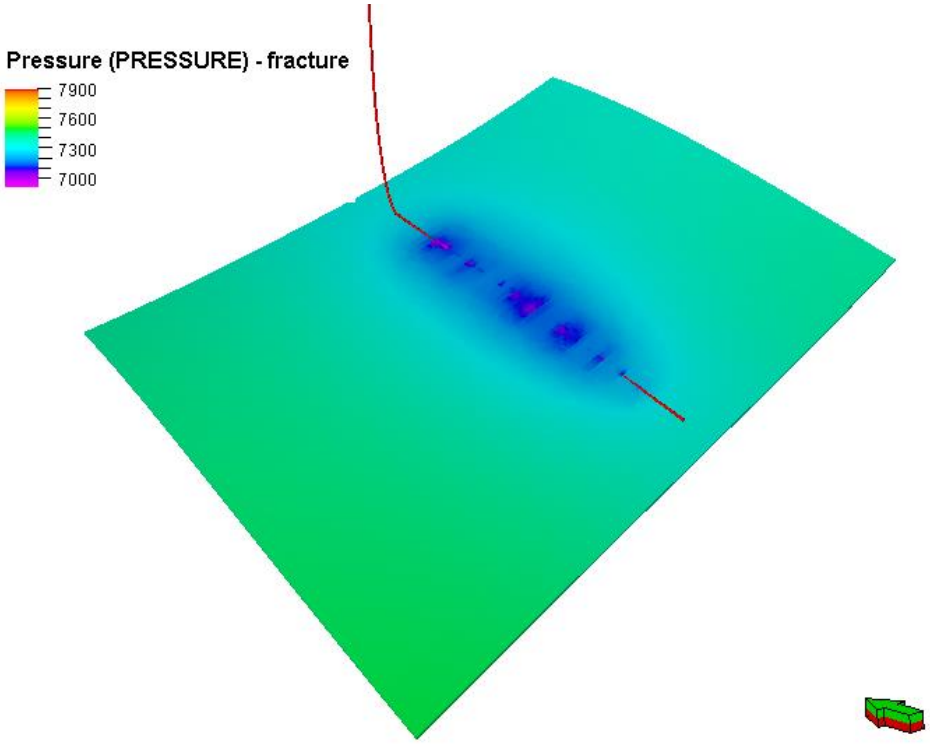

Figure 28. Fracture pressure profile after two years of production (Case B1).

Typical shale wells exhibit a high initial production rate, followed by a sharp decline (50-70%) within the first year of production. As fluids are produced, fracture permeability decreases due to an increase in fracture closure stress. In order to understand the obtained results and improve the simulation model, multiple sensibilities concerning rock compaction tables and natural fractures porosity and permeability, among other variables, were performed. Figure 29 shows the effect of fracture compaction and natural fracture model permeability on well production profile (case B1). Evaluated scenarios are described in Table 13. Despite all efforts, it was not possible to capture the typical shale production profile in any of the simulation runs.

Table 13. Description of the evaluated scenarios for Case B1.

B1	Preliminary oil production profile as shown in Figure 26
B1_TM50	Hydraulic fracture's transmissibility multiplier in the compaction table is reduced by 50%
B1_NF50	Natural fracture model permeability is reduced by 50%
B1_NF25	Natural fracture model permeability is reduced by 75%

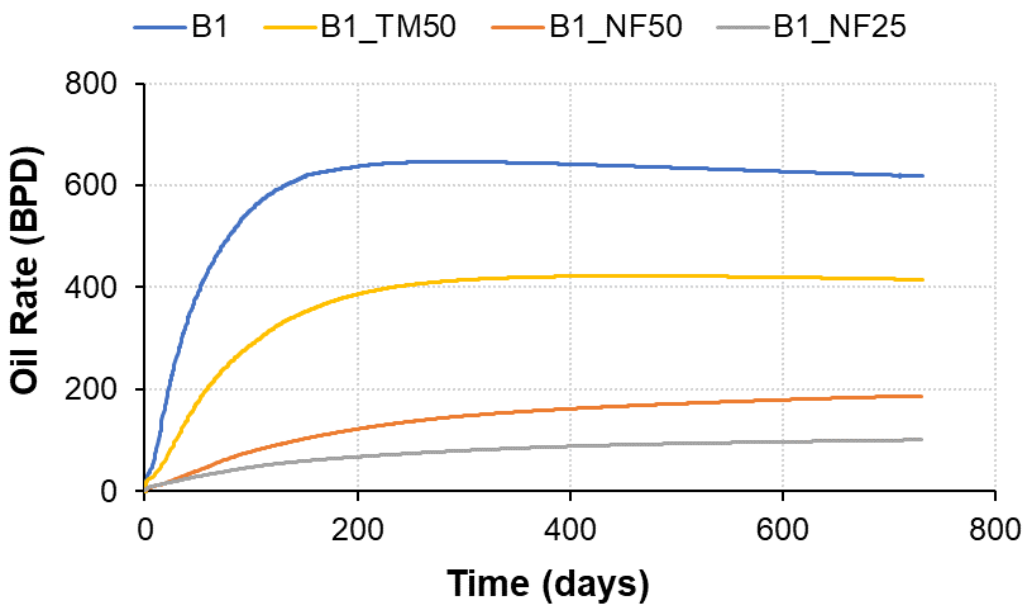

Figure 29. Effect of fracture compaction and natural fracture model permeability on oil production profile (Case B1).

Chapter 6: Discussion/Limitations

The methodology presented in Chapter 3 enabled the characterization and modeling of the Woodford shale and could be easily adjusted to model other unconventional plays. The 3D static model resulted in a reliable representation of the Woodford and its adjacent formations within the study area. Stratigraphic variation and estimated petrophysical and geomechanical properties agreed with previous studies, outcrop interpretations, and laboratory measurements. It is important to mention that the subsurface data used for this study was in the form of raster logs, so previous digitalization work had to be done.

Additionally, most of the available gamma-ray logs do not register values greater than 300 gAPI. Therefore, during the lithofacies classification process, those intervals without gamma-ray records were assumed to be within the same rock type. It is recommended to refine the lithofacies classification by including more lithology indicator logs, such as photoelectric absorption (Pe) and spontaneous potential (SP).

Results of the static model provided a good representation of the main stratigraphic and geomechanical variability of each member of the Woodford: a more brittle upper zone, more ductile lower zone, and a middle zone with an intermediate brittle/ductile behavior. However, adding more information, such as seismic and production data during the reservoir characterization stage would increase the confidence on the static reservoir model and would allow further understanding of the factors controlling the hydraulic fracture propagation and subsequent hydrocarbon production.

The hydraulic fracture modeling workflow introduced in Chapter 4 provided useful insights into the size and characteristics of the SRV surrounding the hydraulically fractured horizontal well by using the geomechanical model from Chapter 3 as a constraint in the stimulation treatment

design, and to improve the asymmetric fracture characterization. Examination of important design parameters, such as pore pressure gradient, pressure-dependent leakoff coefficient, and proppant type, revealed the importance of incorporating uncertainty evaluation regarding unknown variables in the model. Total stress and fluid leakoff have a significant effect on fracture propagation and therefore, in completion efficiency. Stress differences within and between formations also control the vertical growth of fractures.

This study results proved that fractures in the Woodford could grow vertically, leading to communication and possible fluid production from the Sycamore as well. Particularly, if the landing zone is within the more brittle section of the middle Woodford, where stresses tend to decrease upward, and if the leakoff due to pre-existing fissures opening is small. Fracture conductivity showed to be highly dependent on stress and proppant type and concentration. It's worth mentioning that the SRV size and induced fracture conductivity can also be influenced by the pumping schedule and stress shadowing between fracture clusters and stages. Though in this study, for the sake of simplicity, the same pumping schedule was used for all cases, and stress shadowing was only considered between clusters. The pumping schedule was defined according to common completion practices in the Woodford.

The approach presented in Chapter 5 enabled the integration of the hydraulic fracture model with the geologic model. SRV size and fracture conductivity were represented by transmissibility multipliers. The dual-porosity model allowed to account for the volume of hydrocarbons stored within both the matrix and fractures and the fluid's preferential flow through the high conductivity fractures. Though, while the simulation deck was set up according to common unconventional reservoir simulation practices, the outcome was unexpected. Well production profile depicted little initial oil production, small decline rate, and a constant gas-oil

ratio that appeared not to be affected by the very low bottom hole pressure. These results did not match with the typical production profile seen in unconventional wells. It is also important to mention that production data, for the study area, was unavailable. Multiple sensitives regarding rock compaction tables, porosity, and permeability of natural fractures, initial fluids saturation, grid model size, among others, were performed to understand and improve the well's production profile. Still, outcomes did not fulfill the expectations. Additional research about coupled reservoir simulation with geomechanics is recommended.

Chapter 7: Conclusions

This study illustrates the importance of reservoir characterization and geomechanical modeling for hydraulic fracture design and well performance evaluation. Some of the main takeaways are listed next:

- Integration of subsurface data and core/outcrop interpretations enable the reliable representation of the lateral and vertical heterogeneity of the Woodford shale and its neighboring formations in the study area.
- The static model showed the stratigraphic variability that exists within the Woodford. The lower member contains the most clay-rich and ductile lithofacies. The middle member has an intermediate proportion between clay- and quartz-rich lithofacies exhibiting an upward increase of brittleness. The upper member comprises the most quartz-rich and brittle lithofacies.
- The hydraulic fracture modeling revealed that total stress, pressure-dependent leakoff, and proppant type have a significant effect on fracture propagation, growth, and conductivity.
- Longer fractures with less height are created under lower stress when the pore pressure gradient is 0.44 psi/ft. The opposite occurs at higher stress, where fractures tend to be shorter and grow more in the upward direction.
- The upward growth of fractures, even beyond the Woodford, is influenced by the decreasing upward trend in stress around the landing zone and the pressure-dependent leakoff.

- Fractures extend more into the Woodford formation when the pressure-dependent leakoff is low. Incrementing the PDL coefficient from 0.0002 to 0.002 psi^{-1} reduces the size of the effective SRV in about 70%.
- Fracture conductivity is highly impacted by closure stress and type of proppant. More crush-resistant proppant, such as bauxite, exhibit higher average conductivity compared to curable resin-coated sand. But, an increase in stress, with the same type of proppant, reduces its conductivity by almost 50%.

Nomenclature

D_{tv}	true vertical depth, ft
E	Young's modulus, Mpsi
G	Bulk modulus, Mpsi
K	Shear modulus, Mpsi
S_{hmax}	horizontal maximum principal stress, psi
S_{hmin}	horizontal minimum principal stress, psi
V_p	compressional wave velocity, ft/s
V_s	shear wave velocity, ft/s
V_{sh}	shale content, fraction
α_h	horizontal Biot's poroelastic constant, dimensionless
α_v	vertical Biot's poroelastic constant, dimensionless
γ_{ob}	overburden stress gradient, psi/ft
γ_p	pore pressure gradient, psi/ft
ε_x	regional horizontal strain, microstrains
ν	Poisson's ratio, dimensionless
ρ_f	drilling fluid density, g/cm^3
ρ_{ma}	grain matrix density, g/cm^3
ρ_{RHOB}	bulk density, g/cm^3
σ_t	regional horizontal tectonic stress, psi
ϕ_D	density porosity, fraction
$\phi_{D\,sh}$	shale density porosity, fraction

ϕ_e	effective porosity, fraction
ϕ_N	neutron porosity, fraction
$\phi_{N\,sh}$	shale neutron porosity, fraction

References

Abouelresh, M. O., and Slatt, R. M. (2011). Shale Depositional Processes: Example from the Paleozoic Barnett Shale, Fort Worth Basin, Texas, USA. *Central European Journal of Geosciences, 3*(4), 398–409.

Ahmed, I., Oza, S., Vargas-Silva, S., Poludasu, S., Paryani, M., Attia, B., … Ouenes, A. (2017). Cracking the Code of Unconventional Reservoir Simulation. In *SPE Kingdom of Saudi Arabia Annual Technical Symposium and Exhibition*. Society of Petroleum Engineers.

Ataman, O. (2008). *Natural Fracture System in the Woodford Shale, Arbuckle Mountains, Oklahoma*. *Master's thesis*. Oklahoma State University, Oklahoma City, OK.

Badra, H. (2011). *Field Characterization and Analog Modeling of Natural Fractures in the Woodford Shale, Southeast Oklahoma*. *Master's thesis*. University of Oklahoma, Norman, OK.

Barree and Associates LLC. (2017). GOHFER® 3D User Manual. Retrieved from https://barree.net/gohfer.html

Barree, R. D. (2016). *Fracture Conductivity and Cleanup in GOHFER®*. Retrieved from www.gohfer.com

Becerra, D. M. (2017). *Integrated Geological Characterization at the Bed Scale of the Woodford Shale at the I-35 Outcrop, Southern Oklahoma*. *Master's thesis*. University of Oklahoma, Norman, OK.

Bhuyan, K., and Passey, Q. R. (1994). Clay Estimation from GR and Neutron-Density Porosity Logs. *SPWLA 35th Annual Logging Symposium*.

Brito, R. (2019). *The Woodford Shale in the Marietta Basin (Oklahoma and North Texas)*. *Doctoral dissertation*. University of Oklahoma, Norman, OK.

Callner, S. A. (2014). *An Integrated Approach to Understanding Sedimentary Structures and Depositional Processes in Devonian-Mississippian Black Shale: The Woodford Shale and Associated Strata in the Southern Midcontinent*. *Master's thesis*. Oklahoma State University, Oklahoma City, OK.

Cardott, B. J. (2012). Thermal Maturity of Woodford Shale Gas and Oil Plays, Oklahoma, USA. *International Journal of Coal Geology*, *103*, 109–119.

Castagna, P., Batzle, M. L., and Eastwood, R. L. (1985). Relationships between compressional-wave and shear-wave velocities in clastic silicate rocks. *Geophysics*, *50*(4), 571–581.

Clark, N. E., and Wall, L. J. (2007). Development of Sycamore Sandstone Sholom Alechem Field, Stephens and Carter Counties, Oklahoma. *Journal of Petroleum Technology*, *30*(01), 35–42.

Duarte, D. (2018). *Rock Characterization and Stratigraphy of the Mississippian Strata,*

Meramec/Sycamore. Merge play, Central Oklahoma. *Master's thesis*. Univerisity of Oklahoma, Norman, OK.

Galvis-Portilla, H. A. (2017). *Detailed Lithostratigraphic Characterization and Sequence Stratigraphy of a Complete Woodford Shale Outcrop Section in Southern Oklahoma*. *Master's thesis*. University of Oklahoma, Norman, OK.

Ghosh, S. (2017). *Integrated Studies on Woodford Shale Natural Fracture Attributes, Origin, and Their Relation to Hydraulic Fracturing. Doctoral dissertation*. University of Oklahoma, Norman, OK.

Gonzalez, J. W., Perozo, A. E., and Medina, F. X. (2016). Quantification of the Distribution of Initial Water Saturation through Leverett J Function to Calculate Hydrocarbon Reserves Rock. In *SPE Latin American and Caribebean Heavy and Extra Heavy Oil Conference*. Society of Petroleum Engineers.

Grieser, W. V. (2011). Oklahoma Woodford Shale: Completion Trends and Production Outcomes from Three Basins. In *SPE Production Operations Symposium*. Society of Petroleum Engineers.

Gupta, M., Joshi, R., and Kelkar, M. (2005). Dewatering of Hunton Reservoir: What Makes it Work? In *SPE Production Operations Symposium* (pp. 1–10). Society of Petroleum Engineers.

Gupta, N., Rai, C. S., and Sondergeld, C. H. (2013). Petrophysical Characterization of the Woodford Shale. *Petrophysics*, *54*(04), 368–382.

Hai, Q., Ying, L., Chuande, Z., Liancheng, R., Qinwen, W., Yancang, L., and Jun, H. (2017). The Characteristics of Hydraulic Fracture Growth in Woodford Shale, the Anadarko Basin, Oklahoma. In *SPE/IATMI Asia Pacific Oil & Gas Conference and Exhibition* (p. 9). Society of Petroleum Engineers.

Higley, D. K., Cook, T. A., and Pawlewicz, M. J. (2018). Petroleum Systems and Assessment of Undiscovered Oil and Gas in the Anadarko Basin Province, Colorado, Kansas, Oklahoma, and Texas—Woodford Shale Assessment Units, Chapter 6. *U.S. Geological Survey Digital Data Series DDS–69–EE*, 24. Retrieved from https://pubs.usgs.gov/dds/dds-069/dds-069-ee/

Hu, K., Schmidt, A., Barhaug, J., Wong, J., Tian, J., and Hall, B. E. (2015). Sand, Resin-Coated Sand or Ceramic Proppant? The Effect of Different Proppants on the Long-Term Production of Bakken Shale Wells. In *SPE Annual Technical Conference and Exhibition*. Society of Petroleum Engineers.

Jensen, C. L., Lee, S. H., Milliken, W. J., Kamath, J., Narr, W., Wu, H., and Davies, J. P. (1998). Field Simulation of Naturally Fractured Reservoirs Using Effective Permeabilities Derived From Realistic Fracture Characterization. In *SPE Annual Technical Conference and Exhibition* (pp. 157–170). Society of Petroleum Engineers.

Jing Zhang. (2016). *Comprehensive Reservoir Characterization of The Woodford Shale in parts*

of Garfield and Kingfisher Countyies, Oklahoma. *Master's thesis*. University of Oklahoma, Norman, OK.

Jolliffe, I. T. (2002). *Principal Component Analysis* (2nd ed.). New York: Springer.

Lambert, M. W. (1993). Internal Stratigraphy and Organic Facies of the Devonian-Mississipian Chattanooga (Woodford) Shale in Oklahoma and Kansas - Chapter 11. In *Source Rocks in a Sequence Stratigraphic Framework* (pp. 163–176). Kansas Geological Survey.

McCullough, B. (2014). *Sequence-Stratigraphic Framework and Characterization of the Woodford Shale on the Southern Cherokee Platform of Central Oklahoma*. *Doctoral dissertation*. University of Oklahoma, Norman, OK.

McKeon, M. (2011). *Horizontal Fracturing in Shale Plays*. Retrieved from http://www.thepttc.org/workshops/eastern_062111/eastern_062111_McKeon.pdf

Milad, B. (2019). *Integrated Reservoir Characterization and Geological Upscaling for Reservoir Flow Simulations of the Sycamore/Meramec and Hunton Plays in Oklahoma*. *Doctoral dissertation*. University of Oklahoma, Norman, OK.

Miller, J. (2018). *Regional Stratigraphy and Organic Richness of the Mississippian Meramec and Associated Strata, Anadarko Basin, Central Oklahoma*. *Master's thesis*. University of Oklahoma, Norman, OK.

Molinares-Blanco, C., Matemilola, M., Zhang, J., Galvis, H., Becerra, D., Infante, L., and Slatt, R. (2017). Reservoir Optimization, Mechanical Stratigraphy, and Stress Field Orientation in the Woodford Shale SCOOP (South Central Oklahoma Oil Province) Play: A Case Study from Grady County , Oklahoma. *American Association of Petroleum Geologists, Search and Discovery Article # 10984*.

Molinares, C., Slatt, R. M., and Sierra, R. (2016). Effect of anisotropy (lamination) on rock fracability for Vertical Transverse Isotropic (VTI) unconventional reservoirs, a comparison between upper (Highstand System Tract - HST) and middle (Transgressive System Tract - TST) Woodford Shale. In *SEG International Exposition and 86th Annual Meeting* (pp. 485–489). Society of Exploration Geophysicists.

Nelson, P. H., and Gianoutsos, N. J. (2014). Present-Day Overpressure and Paleopressure Indicators in the Greater Anadarko Basin, Oklahoma, Texas, Kansas, and Colorado, Chapter 8. *U.S. Geological Survey Digital Data Series DDS–69–EE*, 28. Retrieved from https://pubs.usgs.gov/dds/dds-069/dds-069-ee/

Peza, E., Kvale, E., Hand, R., Harper, W., Jayakumar, R., Wood, D., … Ganpule, S. (2014). 3-D Integrated Workflow for Understanding the Fracture Interference and its Impact into the Gas Production of the Woodford Shale. In *Unconventional Resources Technology Conference* (pp. 1–26). Society of Petroleum Engineers.

Phelps, R. E. (1993). Lithology-Dependent J-Functions and Relative Permeabilities. In *SPE Middle East Oil Technical Conference & Exhibition* (pp. 525–536). Society of Petroleum

Engineers.

Rider, M. (2000). *The Geological Interpretation of Well Logs* (2nd ed.). Rider-French Consulting Ltd.

Ryan, B. E. (2017). *Petrophysical Properties of the Woodford Formation in the Ardmore Basin in Oklahoma, U.S.A. Master's thesis*. University of Texas at Arlington.

Sierra, R., Tran, M. H., Abousleiman, Y. N., and Slatt, R. M. (2010). Woodford Shale Mechanical Properties And the Impacts of Lithofacies. In *44th U.S. Rock Mechanics Symposium and 5th U.S.-Canada Rock Mechanics Symposium*. American Rock Mechanics Association.

Slatt, R. M. (2011). Important Geological Properties of Unconventional Resource Shales. *Central European Journal of Geosciences*, *3*(4), 435–448.

Slatt, R. M. (2013). *Stratigraphic Reservoir Characterization for Petroleum Geologists, Geophysicists, and Engineers - Origin, Recognition, Initiation, and Reservoir Quality*. *Developments in Petroleum Science* (2nd ed., Vol. 61). Norman, Oklahoma: Elsevier.

Slatt, R. M., Mccullough, B., Molinares, C., Baruch, E., and Turner, B. (2015). Paleotopographic and Depositional Environment Controls on " Sweet Spot " Locations in Unconventional Resource Shales : Woodford and Barnett Shale Examples : Part 2 *. *American Association of Petroleum Geologists, Search and Discovery Article #80467*.

Terracina, J. (2011). Effects of Proppant Selection on Shale Fracture Treatments. *Journal of Petroleum Technology*, *63*(05), 26–29.

Torres-Parada, E. J., Sinha, S., Infante-Paez, L. E., Slatt, R. M., and Marfurt, K. J. (2018). Seismic to Simulation : Woodford Shale Case Study in Oklahoma , USA. In *Unconventional Resources Technology Conference* (pp. 1135–1151). Society of Exploration Geophysicists, American Association of Petroleum Geologists, Society of Petroleum Engineers.

Turner, B. W. (2016). *Utilization of Chemostratigraphic Proxies for Generating and Refining Sequence Stratigraphy Frameworks in Mudrock and Shales*. *Doctoral dissertation*. University of Oklahoma.

Vulgamore, T., Wolhart, S., Mayerhofer, M., Clawson, T., and Pope, C. (2018, March). Hydraulic Fracture Diagnostics Help Optimize Stimulations of Woodford Shale Horizontals. *American Oil & Gas Reporter*.